# Accuracy and suitability of satellite-based retrieval products for operational precipitation nowcasting in Ghana

**Master Thesis by Vera Glas**

Faculty of Engineering Technology, Water Engineering and Management, University of Twente

25-04-2024

Supervisors: dr.ir M.J. Booij (University of Twente), dr. ing T.H.M. Rientjes (University of Twente), ir. D. Lugt (HKV), dr.ir. R.T.W.L. Hurkmans (HKV).

## Abstract

There is an urgent need for reliable now- and forecasting of (extreme) precipitation on the African continent. Early warning for extreme rainfall contributes to disaster preparedness and can decrease the associated risks. Precipitation data with a high temporal and spatial resolution is of high value for hazard models, especially flash floods. For short lead times (0-6h), nowcasting approaches that extrapolate ground-radar observations are commonly applied in practice. However, operational nowcasting efforts on the African continent are hindered due to the limited availability of ground-radar data. The increasing availability and resolution of satellite-based retrieval products show the potential to partly overcome the need for ground-based radar stations. This study addresses the accuracy and suitability of satellite-based retrieval products for operational precipitation nowcasting in Ghana.

The high spatio-temporal resolution of Meteosat data (15 minutes and 3 km) in combination with its relatively short latency of 45 minutes offers potential for operational nowcasting initiatives. This study focusses on the accuracy and applicability of the MSG-CPP retrieval products (infrared & visual). First, the accuracy of the retrieval products is examined using ground measurement data from 19 stations of the Trans-African Hydro-Meteorological Observatory (TAHMO) organization. It is concluded that the MSG-CPP retrieval products significantly overestimate the measured precipitation intensities. On a 15-minute temporal resolution, the probability of detecting precipitation is 49% for the IR-based MSG-CPP retrieval product and 81% for the visual retrieval product. Moreover, the visual product has a higher false alarm ratio which significantly influences the associated critical success indices of 0.20 and 0.19. Additionally, the detection capabilities for peak precipitation are examined. In this study peak precipitation is defined as the 95% percentile precipitation intensity of the TAHMO measurements. The associated probability of detection is 19% for the IR product and 39% for the visual one. The statistical patterns in the MSG-CPP and TAHMO data are so different that bias correction seems unsuitable.

To study the MSG-CPP retrieval performance in relation to other satellite-based precipitation products, a comparative analysis is made using precipitation data from CMORPH and GPM IMERG. This analysis is performed for eight heavy precipitation events in the Odaw basin region. The results show that all satellite precipitation products present higher rainfall depths than the TAHMO measurements. This observation raises questions about the accuracy of the TAHMO data, which is not validated within the scope of this research. The start, peak, and end times of the precipitation events show clear similarities and deviate up to approximately 1.5 hours between datasets. Moreover, the retrieval products with longer latencies (IMERG Final & CMORPH), do not show a higher correspondence with ground observations compared to the products with short latencies (MSG-CPP IR and IMERG Early). To analyze the usability of satellite-based precipitation products for operational nowcasting purposes, the open-source Python nowcasting package Pysteps is utilized. The deterministic S-PROG method is applied to analyze the nowcasting skill using the MSG-CPP IR retrieval product for 116 precipitation events in Ghana. Median skillful nowcast performances are observed for 45-, 90-, 120- and 135 minutes of lead times for the respective spatial scale levels of 9-, 60-, 180-, and 300 km. Furthermore, it is observed that the S-PROG nowcast method tends to extrapolate precipitation patterns in the input data. This phenomenon affects the accuracy of the nowcasted precipitation intensities.

This study aims to underline the potential of satellite-based precipitation nowcasting while being transparent concerning the existing limitations and remaining uncertainties. By solely utilizing open data sources, this research contributes to open access of precipitation now- and forecasts. These research efforts are in line with the Early Warning for All initiative as called for by the United Nations Secretary-General in 2022.

# 1. Introduction

Many areas in Africa are subject to extreme rainfall events which cause large social-economic disturbances. Due to climate change, the intensity and frequency of these events are expected to increase (Codjoe & Atiglo, 2020). Early warning for extreme rainfall contributes to disaster preparedness and can decrease the associated risks (United Nations, 2023). Moreover, in many hydrological models, precipitation data is the largest source of model uncertainty. Consequently, increasing the accuracy of rainfall data is highly relevant to enlarge the reliability of flood and river discharge models and the associated risk-informed decision-making processes (Kobold & Sušelj, 2005). For flash flood early warning, nowcasting techniques are required. For the scope of this research, nowcasting is defined as the process of providing weather forecasts that extend from the present to a time window up to six hours into the future. Traditional nowcasting approaches use a detailed observation of the current (initial) state which is subsequently extrapolated to derive a forecast for the near future (Smith & Austin, 2000). Commonly, ground-based radar data is used as observational data and the associated nowcast data shows reliable performance indicators up to approximately three hours of lead time (Imhoff et al., 2020).

On the African continent, the availability of ground-based radar stations is limited, which hinders the production of reliable precipitation now- and forecasts (Wismans, 2023). Increasing computational power and the growing spatial and temporal resolution of satellite imagery offer possibilities for nowcasting without the need for ground-based radar data. A remaining challenge is that many satellite-based retrieval products have latencies that make them unsuitable for operational nowcasting. Since 2012, the Dutch Royal Meteorological Institute (KNMI) has run and freely published rainfall data based on the Meteosat Second Generation, Cloud Physical Properties (MSG-CPP) algorithm. This data has a latency of 45 minutes and shows a large potential to be used for nowcasting. This research explores and evaluates the suitability of the MSG-CPP rainfall retrieval product for detecting and nowcasting precipitation in Ghana. Ghana is selected as a case-study area due to the availability of ground measurement stations and the expressed interest of local meteorological organizations in nowcasting products. Moreover, the MSG-CPP data is compared with two other open available satellite-based precipitation products, namely CMORPH and GPM IMERG. The CMORPH and GPM IMERG datasets are selected based on their small observation interval (30 min). Moreover, they are frequently used in climatological and hydrological studies for areas with limited ground-radar coverage (Atiah et al., 2020; Joyce et al., 2004; Kawo et al., 2021). The CMORPH and GPM IMERG products themselves are not considered suitable for operational nowcasting due to their long latencies.

## 1.1. Precipitation retrieval from satellite imagery

Translating raw satellite data to precipitation estimates is a complex challenge for which a variety of instruments and algorithms have been developed. A first approach to retrieve rainfall uses passive microwave sensors. These sensors measure radiation which is emitted by the earth's surface at multiple microwave frequencies. The observed radiation is expressed as brightness temperature (Kummerow, 2020). By using multi-frequency precipitation retrieval algorithms, the relationship between microwave signals and precipitation intensity is determined. An advantage of passive microwave sensors is that they enable continuous monitoring throughout all hours of the day. A disadvantage is that microwave sensors have limited sensitivity to light precipitation quantities, for example, drizzle (Prigent, 2010; Kikuchi et al., 2022). Another approach for continuous rainfall retrieval utilizes infrared satellite data. Infrared sensors measure for different wavelengths the radiation of the atmosphere and use this to determine the cloud-top temperature (Prigent, 2010). A disadvantage is that infrared data provides less accurate estimates of precipitation rates due to the lack of detailed information concerning, for example, liquid particle density in the atmosphere. Moreover, classification between diverse types of precipitation, such as rain and snow is challenging (Varma, 2018; Beusch et al., 2018). Another approach for rainfall retrieval uses visible light sensors on satellites which capture sunlight scattering caused by the earth's surface and clouds. This data is valuable for determining cloud cover and the presence of precipitation particles. Visual light data is particularly useful for the visual assessment of storm systems (Prigent, 2010). Nevertheless, the approach is daylight-dependent and faces difficulties in determining precise quantitative rainfall rates (Varma, 2018).

The MSG-CPP retrieval product is derived from data from the Meteosat satellite. Meteosat is the name of a series of geostationary weather satellites of the European Space Agency (ESA) and EUMETSAT which cover the European and African continent. For weather nowcasting purposes the most important instrument on the Meteosat satellite is the SEVIRI (Spinning Enhance Visible and Infrared Imager). The advantage of using data from a

geostationary satellite is the high temporal resolution and short latency (15 min and 45 min) of the data. However, due to its larger distance to Earth, passive microwave sensors are not applicable. The IMERG and CMORPH precipitation retrieval products both primarily utilize passive microwave sensors from various low earth orbit satellites and have a temporal resolution of 30 minutes (Tan et al., 2019; Joyce et al., 2004). Additionally, CMORPH has a spatial resolution of 8 km and IMERG of 10 km.

## 1.2. Current practices for weather predictions

To predict upcoming weather events there are various methods applied in practice. For nowcasting, optical flow and machine learning methods can be applied. When producing weather predictions with lead times of more than six hours, the term forecasting is applicable. Weather forecasts are commonly produced by using Numerical Weather Prediction (NWP) models. Additionally, there is a growing research field focusing on the development of seamless weather models that blend nowcast and NWP data. In table 1 the main advantages and disadvantages of each of the mentioned methods are presented.

***Table 1 Overview of existing weather prediction methods***

| Nowcasting method | Advantages | Disadvantages |
|---|---|---|
| **Optical flow** | - Industry-standard<br>- Skillful for short lead times (0-3h) | - Limited skill in representing convective precipitation<br>- Large performance variability related to e.g., season and geographic location |
| **Machine learning** | - Computationally efficient after training<br>- Data-driven model so no need for assumptions such as Lagrangian persistence<br>- Skillful for short lead times (0- 2h) | - Requires training data of high quality and preferably in large volumes<br>- Risk of over-fitting and training data bias<br>- Interpretability can be challenging |
| **Numerical Weather Prediction (NWP) models** | - Can capture non-linear growth and decay of precipitation<br>- Skillful for longer lead times | - High computational demands<br>- Requires high-resolution spatial and temporal data<br>- High sensitivity to initial conditions<br>- Long spin-up times (3-6h) |
| **Blended approaches** | -Potential to create a seamless nowcasting model | - Risk of moving to climatological mean<br>- Inconsistencies in output data |

***Optical flow methods***

Nowcasting approaches based on the extrapolation of observations are executed in two steps. First, recent observations are analyzed to determine motion fields. Secondly, an advection scheme is applied to extrapolate the last observation along the determined motion vector (Pierce et al., 2012). A core assumption used in extrapolation nowcasting methods is the existence of Lagrangian persistence. Lagrangian persistence states that rainfall intensity and motion fields are stationary over time. Extrapolation-based nowcasting methods show a large skill dependency on event duration, spatial scale, season, and location. The Lagrangian persistence limits the extrapolation-based nowcasting abilities for dynamic, heavy, and localized rain events, such as convective precipitation. For small convective rainfall events, skillful lead times are limited to 30 minutes. Larger scale persistent precipitation events show skillful lead times of two hours and only continental scale stratiform events are reliably nowcasted with lead times of six hours (Imhoff et al., 2023; Ayzel et al., 2019). Moreover, errors in rainfall nowcasts increase significantly with rainfall intensity and spatial variability (Imhoff et al., 2022).

***Machine learning models***

Over the past years, machine learning methods for nowcasting purposes have increased in popularity. Machine learning models do not rely on physical equations and can therefore overcome the need for assumptions, such as the Lagrangian persistence. Shi et al., (2015) developed a convection nowcasting method using a convolutional Long Short-Term Memory (ConvLSTM) algorithm. Convolutional Neural Network (CNN) models show nowcasting skills that outperform traditional radar extrapolation-based methods (Shi et al., 2015; Shi et al., 2017). Moreover, Foresti et al., (2019) used an Artificial Neural Network (ANN) to capture the nonlinear relationships between growth and decay of precipitation. The study concluded that average long-term growth and decay patterns are effectively reproduced. However, real-time prediction is more challenging. In 2021 the DeepMind department of Google presented the Deep Generative Model of Radar (DGMR) for precipitation nowcasting. Generative models learn from the statistical relations in their training data and subsequently generate data samples based on learned distributions. Ravuri et al., (2021) compared the results of the DGMR model with the nowcasting performance of existing extrapolation-based methods such as S-PROG and STEPS (Pulkkinen et al., 2019). Quantitative performance indicators showed that the DGMR model outperforms the S-PROG and STEPS methods from a spatial accuracy perspective.

Nevertheless, it is important to remark that the accuracy of DGMR models decreases significantly with lead times of more than 90 minutes. Moreover, the DGMR model showed difficulties in predicting isolated showers. Overall, the quality of a machine learning model highly depends on the quality and available amount of training data.

***Numerical Weather Prediction (NWP)***

NWP models use dynamic and physically based equations that explain atmospheric conditions to predict future weather conditions. The advantage of NWP models is the ability to capture the non-linear evolution of weather phenomena, such as the growth and decay of precipitation. To apply NWP models for short lead times, data assimilation of high spatial and temporal resolution is key (Pierce et al., 2012). NWP models with a horizontal resolution of 1-4 km enable convective-permitting simulations (Sun et al., 2014; Clark et al., 2009; Weisman et al., 2008). The predictive skill of NWP models exceeds the nowcasting performances of extrapolation methods after the first hours of lead time (Sun et al., 2014).

Nevertheless, NWP models face several challenges. Firstly, they are highly sensitive to their initial conditions and the definition of realistic boundary conditions is difficult. Additionally, NWP models are computationally heavy and cope with large spin-up times, which limits their updating frequency. For convective-permitting NWP models, spin-up times are commonly between three and six hours (Imhoff et al., 2020;Pierce et al., 2012;Sun et al., 2014). Ongoing developments using rapid updating cycles and high-resolution data assimilation techniques contribute to the forecasting performances of NWP models (Sun et al., 2014; Payne, 2017; Honda et al., 2022). Nevertheless, the remaining latency of several hours between model initialization and forecasting data limits the applicability of NWP models for short lead times (Imhoff et al., 2023).

For operational (global) forecasting purposes there are practically two NWP models available, namely the model of the European Center for Medium-Range Weather Forecasts (ECMWF) and the Global Forecasting System (GFS). ECMWF is a nonhydrostatic weather model. This means that altitude is an important input parameter in the model setup. The GFS model is hydrostatic, this means that the vertical acceleration of air is not derived explicitly. Instead of altitude, GFS uses atmospheric pressure which reduces the computational demands. Additionally, ECMWF has a spatial resolution of 14 km, whereas the GFS model has a spatial resolution of 27 km. Both models have a temporal resolution of 1 hour for the first days of lead time. The updating frequency of the ECMWF model is 12 hours, whereas the GFS model has an updating frequency of 6 hours (National Center for Environmental Information, 2023;ECMWF, 2023). Numerous studies have been conducted which compare the accuracy of both models (Medina et al., 2019; Hamill et al., 2008;Kuznetsov, 2023). In general, the literature results state that ECMWF is consistently better. This is likely due to the non-hydrostatic character. Nevertheless, the GFS model shows higher skills in forecasting severe and extreme weather phenomena (Kuznetsov, 2023).

***Blended nowcasting approaches***

Different weather prediction methods show skillful performances for varying lead times. For short lead times, extrapolation and machine learning techniques are most skillful. NWP models show a higher accuracy for longer lead times. Blended nowcasting approaches aim to combine the different methods to create a seamless model that is applicable for varying lead times. Blending requires a reprojection of various models onto the same grid and the creation of a common temporal frequency. Subsequently, weights can be given to each data source to create a blended merge of input sources (Vannitsem et al., 2021). These weights can be adjusted based on various factors, such as lead time and spatial scale. In literature, a variety of blending techniques is described. Examples of blending algorithms are the hyperbolic tangent curve (HTW), the critical success index (CSIW) and the salient cross dissolve (Sal CD) (Radhakrishnan & Chandrasekar, 2020; Nerini et al., 2019). Recently, Imhoff et al., (2023) created an adaptive and scale-dependent blended nowcasting approach. The new method shows similar to better performances than individual radar extrapolation or NWP-based approaches. An added value is especially recognized for the first forecasting hours and the representation of instantaneous rainfall rates. A risk of using blending methods is the trend to move to a climatological mean. When using various input sources, inconsistencies may arise between the location and spatial scale of a precipitation feature. In a blended output this can lead to unrealistic output, for example, abrupt changes in weather conditions (Vannitsem et al., 2021).

### 1.3. The Republic of Ghana, case-study area

The Republic of Ghana is a country in West Africa with a population of 34.1 million in 2023. Ghana has a tropical climate which is strongly influenced by the West African monsoon winds (World Bank Group, 2023). On an annual basis, Ghana faces floods. Besides their immediate destructive effects, floods have negative consequences on the social and economic development in the region

(Mensah & Ahadzie, 2020). In the face of climate change, extreme weather events in Ghana are expected to increase. The dry seasons will become dryer and rainfall quantities during the rainy season are expected to increase (Logah et al., 2014). Ghana is selected as a case-study region because of its availability of rainfall observation data from the Trans-African Hydro-Meteorological Observatory (TAHMO).

The responsible institution for weather monitoring and forecasting is the Ghana Meteorological Agency (GMET) and for flood management the Hydrological Services Department (HSD). The National Disaster Management Organization (NADMO) is responsible for formulating and distributing early warning messages and potential crisis response. The current applied flood forecasting system in Accra is solely based on rainfall monitoring. GMET runs a Weather Research and Forecasting (WRF) model with a resolution of 9 km, an updating frequency of 6 hours, and a lead time of 5 days. Published research that evaluates the quality and accuracy of these current forecasting methods is scares. There have been various initiatives that address precipitation now- and forecasting for Ghana. A collaboration between HKV and the Royal Dutch Meteorological Institute (KNMI) led to the development of the RAINSAT Convolutional Neural Network nowcasting model (rainsat.net) using the MSG-CPP data and the nowcasting method as described by Shi et al., (2017). For the Netherlands, this method showed skillful performances up to three hours of lead time (van der Kooij, 2021). For Ghana, no published research is available which reflects on the accuracy of the RAINSAT nowcasting performance.

An additional nowcasting initiative in Ghana is the Science for Weather Information and Forecasting Techniques (SWIFT) project. The African SWIFT project was active from 2017 to 2022 and was led by the National Centre for Atmospheric Science (NCAS). In the scope of the SWIFT project the FASTA (Forecasting African Storms Application) app was developed. The FASTA app has a lead time of two hours. The app shows great potential; however, no clear performance evaluation has been published. While the original SWIFT plan describes the goal to develop the FASTA app for Ghana, it seems that currently, only a Kenyan version is available.

Furthermore, Aryee et al., (2022) describe the implementation of a nowcasting approach using algorithms of the Nowcasting and Very Short Range Forecasting Satellite Application Facility (NWC SAF) and Meteosat data to improve early warning in Ghana. A performance analysis using 174 events showed a probability of detection of 68% and a false alarm rate of 17%. It is unclear what the current status is of these nowcasting initiatives and to which degree they are operational.

In summary, Ghana is prone to extreme precipitation and (urban) flooding. To mitigate disaster risks, there is a need for reliable now- and forecasting data. There have been various local and international organizations active in the development of now- and forecasting models. These initiatives are promising, however, based on literature research it remains unclear how accurate and operational the different initiatives are.

### 1.4. Research gap

As discussed in section 1.2, the industry standard for nowcasting models is the usage of ground-based radar data. Many areas on the African continent have limited access to ground-based radar data which hinders nowcasting and early warning initiatives. In Ghana, there have been various initiatives that aimed to compose operational precipitation nowcasting. The quality and current status of these nowcasting initiatives received very little attention in published reporting. This is considered a research gap.

The high spatial-temporal resolution of Meteosat data in combination with its relatively short latency offers the potential for operational precipitation nowcasting without the need for ground radar. Unfortunately, the availability of retrieval algorithms that enable operational nowcasting is limited. KNMI has developed the MSG-CPP rainfall retrieval algorithm which uses Meteosat data as input and provides free and openly available precipitation data. For a long period, very little attention and no published findings were available in which the accuracy of MSG-CPP retrieval products was examined for a country on the African continent. This is considered a significant research gap. Recently, a paper by Bogerd et al., (2024) presented a first comparative analysis of the MSG-CPP products with IMERG and TAHMO data for Ghana. The paper observes significant differences in the precipitation datasets. To the best of our knowledge, there is no research available that analyzed the applicability of the MSG-CPP retrieval products for nowcasting purposes.

When assessing the suitability of satellite-based precipitation products for nowcasting, it is of high value to analyze the differences between available products. Besides the MSG-CPP algorithm, there are, to the best of our knowledge, two other free and openly available satellite-based precipitation products with a spatial and temporal resolution large enough to serve nowcasting. These products are CMORPH (8 km, 30 min) and GPM

IMERG (10 km, 30 min). In literature, there is limited effort to compare the different retrieval products with ground measurement data for precipitation events in Ghana, especially for small temporal scales. Important to note is that the latency of the CMORPH and GPM IMERG products are in first perspective too long for operational nowcasting, for this reason, a focus is given to the MSG-CPP retrieval product, and the CMORPH and IMERG data is used as reference datasets.

### 1.5. Research objective and scope

The main research objective addressed in this paper is as follows;

*Assess the accuracy and suitability of satellite-based precipitation products for precipitation nowcasting in the Republic of Ghana.*

In this research, a focus is given to the MSG-CPP retrieval products (IR and visual). The MSG-CPP products have the lowest latency and highest temporal and spatial resolution of the available satellite retrieval products that are in the public domain. Moreover, the MSG-CPP retrieval products are already used as input for the nowcasting initiative Rainsat.net. In the first research objective, the capabilities of the MSG-CPP algorithm to detect precipitation events in Ghana are examined.

*Subobjective 1: Analyze the capabilities of the MSG-CPP infrared and visual retrieval algorithm to represent observed precipitation events.*

To analyze the suitability of rainfall retrieval products for nowcasting it is important to analyze the correspondence of the various retrieval products with ground-based measurements. Early warning, especially for flash floods, is dominantly produced on a local scale. The second research objective focuses on the spatial extent of a basin and on the representation of historic precipitation events that could cause flash floods.

*Subobjective 2: Compare and evaluate the ability of various satellite-based retrieval products to represent historic heavy precipitation events on a basin scale in Ghana.*

The final research objective aims to assess the suitability of satellite-based retrieval products for nowcasting and reflect on key data characteristics such as latency and temporal resolution.

*Subobjective 3: Evaluate the nowcasting performance of the S-PROG method in Ghana using the MSG-CPP retrieval product as input data and assess its sensitivity to various temporal resolutions.*

## 2. Materials and Methods

### 2.1. Satellite-based precipitation retrieval products

For this study, the satellite-based retrieval products of MSG-CPP, IMERG and CMORPH are used and compared to TAHMO observations. In table 2 the main characteristics of these datasets are presented. In the following paragraphs, a summary is given of the different retrieval algorithms. A more detailed insight concerning the retrieval methodologies can be found in the cited references.

***MSG-CPP retrieval algorithm***

The MSG-CPP (Cloud Physical Properties) algorithm uses data from the geostationary Meteosat satellite as input and consists of four main parts. The first step is the identification of cloud pixels and the determination of cloud top height and temperature. For this first step, the GEO v2018 algorithm is used which is provided by the NWC SAF, an organization of EUMETSAT. Next, the cloud thermodynamic phase, optical thickness, particle effective radius and liquid water path are determined using an algorithm that was developed by Roebeling et al., (2006) and improved by Benas et al., (2017). The algorithm uses backscatter radiation as the main data source and is therefore daylight dependent. The third step in the MSG-CPP algorithm derives surface solar irradiance using an empirical method which is described by Greuell et al., (2013). Finally, the precipitation rate is estimated. For this estimation, a different method is used during the day compared to the night. Precipitation estimates during daytime are derived using the empirical algorithm of Roebeling & Holleman, (2009) and use the cloud

| | MSG-CPP IR | MSG-CPP Visual | IMERG Early | IMERG Final | CMORPH | TAHMO |
|---|---|---|---|---|---|---|
| **Spatial resolution** | 3 km x 3 km | 3 km x 3 km | 10 km x 10 km | 10 km x 10 km | 8 km x 8 km | Point |
| **Temporal resolution** | 15 min | 15 min | 30 min | 30 min | 30 min | 15 min |
| **Latency** | 45 min | 45 min | 4 h | 3 months | 12 months | 1 h |
| **Availability** | Continuous | Daytime | Continuous | Continuous | Continuous | continuous |
| **Data representation** | Pixel | Pixel | Pixel | Pixel | Pixel | Point |
| **Remote vs in situ** | Space | Space | Space | Space + ground | Space | Ground |

***Table 2 Used data sources and attributes***

properties as determined in the second step of the MSG-CPP model.

During night-time precipitation estimates are derived using an algorithm based on infrared brightness temperature. This Nighttime Infrared Precipitation Estimation (NIPE) method is described in the master thesis of Brasjen, (2014). The NIPE method derives a cloud classification. This cloud class subsequently links to precipitation index values that finally lead to precipitation intensities. In 2017 the NIPE algorithm was improved using GPM radar data between April 2014 and March 2015 for calibration. The improved algorithm showed a CSI of 23% during daytime and 22% during nighttime for classifying a satellite pixel as precipitation or non-precipitation. The derived precipitation rates deviated on average by a factor of 3.5 with the GPM radar observations (Brasjen & Meirink, 2017).

The MSG-CPP rainfall retrieval data which is used in this research covers a time series from January 2020 till December 2023. Nevertheless, a data gap occurs starting in February 2021 till March 2022. Consequently, a time series of 35 months of data is used. The visual light-based product is daylight dependent, for Ghana this means that the retrieval data is available between approximately 7:00 AM and 5:30 PM.

***GPM IMERG retrieval algorithm***

The Integrated Mult-satellitE Retrievals for GPM (IMERG) product is the gridded precipitation data from the Global Precipitation Measurement Mission (GPM) and has been developed by NASA (Huffman, 2020). The IMERG retrieval algorithm integrates passive microwave (PMW), infrared and dual-frequency radar data from various low-earth orbiting satellites and is specifically skillful in capturing heavy rainfall events and convective systems (Hou et al., 2014).To blend and calibrate the different data sources a merged Bayesian methodology is used. In this probabilistic method, the uncertainties which are associated with each data source are captured in the joint probability distribution. Subsequently, weight is given to each data source. The weighted probability density function finally composes the IMERG GPM precipitation estimate. The temporal resolution of the IMERG data is 30 minutes.

Apart from satellite-based data sources, IMERG also integrates data from ground-based gauges from the Global Precipitation Climatology Centre (GPCC). IMERG publishes various versions of its retrieval product with varying latencies. The retrieval product with the shortest latency (4h) is the IMERG Early product. The IMERG Early product provides preliminary estimates of precipitation intensities and undergoes minimal post-processing based on ground measurements. Subsequently, there is the IMERG Late product with a latency of 14 hours. The IMERG Late data incorporates more satellite observations and corrections based on ground observations. Finally, the IMERG Final product is made available with a latency of several months. The IMERG Final product is considered the IMERG version with the highest accuracy due to its extensive postprocessing steps for error correction and validation using GPCC gauge data (Li et al., 2021; Tapiador et al., 2020).

Maranan et al., (2020) analyzed the validity of the GPM IMERG data using a mesoscale rain gauge network in the West African Forest Zone. The study observed a high false alarm ratio for low-intensity rainfall. Moreover, the IMERG data tends to overestimate rainfall from weak convective events and underestimate strong mesoscale convective systems. Additionally, the IMERG performances decreased during the dry season. Research by Pradhan et al., (2022) evaluated the performances of GPM IMERG from a global perspective. In line with the conclusions of Dezfuli et al., (2017), substantial performance differences are noticed between regions and climates. In this study, the most recent versions (V06B) of the IMERG Early and IMERG Final retrieval products are used. The IMERG Early data is selected for its relatively small latency, which is of interest in the scope of operational nowcasting. The IMERG Final data is considered to evaluate the effects of post-processing using ground measurements on the IMERG retrieval product.

***CMORPH retrieval algorithm***

The Climate Prediction Center MORPHing Technique (CMORPH) was developed by the National Oceanic and Atmospheric Administration (NOAA) and described by Joyce et al., (2004). As data input the CMORPH algorithm uses infrared data from a geostationary satellite in combination with passive microwave (PMW) data from orbiting satellites. The advantage of using infrared data from geostationary satellites is the constant and reliable temporal and spatial resolution. On the other hand, PMW data provides more information concerning specific precipitation characteristics. By morphing PMW and infrared data, the strengths of both sources are utilized. However, CMORPH data is not corrected using ground measurements. Due to its high spatial (8 km) and temporal resolution (30 min), CMORPH is often applied for weather analyses, especially in data-scarce regions. A study by Atiah et al., (2020) analyzed the accuracy of CMORPH data in relation to various other precipitation datasets and ground measurements in Ghana. The paper concluded an overestimation of low-intensity rainfall and an

underestimation of high-intensity rainfall. Dinku et al., (2010) described that CMORPH shows good performances in capturing convective rainfall.

### 2.2. Trans-African Hydro-Meteorological Observatory (TAHMO) data

The TAHMO organization aims to develop a vast network of inexpensive and robust weather stations across Africa (van de Giesen et al., 2014). The TAHMO weather stations contain a rain gauge with an ATMOS 41 sensor to measure precipitation. The equipment has a diameter of 9.3 cm and consists of a flared hole which creates rainfall drops, of a known size, which are passing a drip counter. Based on the drip counts and the known drop volume, the precipitation volume per time interval is derived. The TAHMO data has a temporal resolution of 15 minutes and a latency of 1 hour. For high-intensity rain, the composed raindrops become smaller. To account for this phenomenon, ATMOS 41 uses an algorithm that considers drip size volumes for varying rainfall intensities. According to the weather station manual, the precipitation measurements have a resolution of 0.017 mm and an accuracy of 5% for measurements in the range of 0-50 mm/h (TAHMO, 2023).

For this research, TAHMO provided access to 25 of their stations in Ghana. After the first inspection, six of these stations were considered unsuitable due to inconsistencies in the data collection. The locations of the remaining 19 stations are presented in figure 1. Moreover, figure 2 shows the data availability of the different stations. In this research, all rainfall observations below 0.1 mm are set at 0 mm.

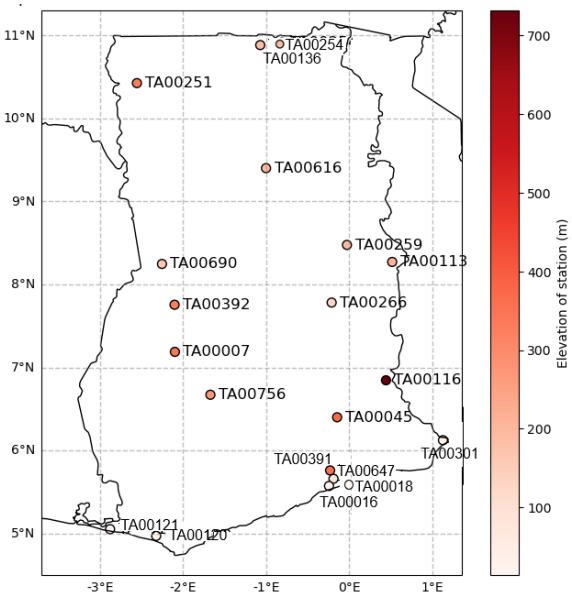


*Figure 1 Map of Ghana with TAHMO stations*

### 2.3. S-PROG nowcasting method

As a nowcasting model, this study uses the deterministic Spectral-PROGnosis (S-PROG) nowcasting model as introduced by Seed (2003). The S-PROG method is selected because it is open-source available and, according to the study of Imhoff et al., (2020), the model outperforms the Rainymotion nowcasting models. To implement the S-PROG model the open-source Python library Pysteps is used. The Pysteps set-up offers a configurable and accessible modular framework for space-time simulations of precipitation (Pulkkinen et al., 2019). As input, the Pysteps framework requires a time series of raster precipitation data. Based on the S-PROG method a stochastic method is developed under the name Short-Term Ensemble Prediction System (STEPS) (Bowler et al., 2006). Nevertheless, in this study, the focus is on the deterministic nowcasting model structure. This choice is made to avoid the addition of stochastic perturbations and therefore simplify the interpretability of the results.

The S-PROG model applies optical flow advection to produce nowcast data. First, a log-normal distribution of rain rates is composed to represent the non-Gaussian distribution of precipitation rates. Subsequently, field advection finds place by estimating the movement of the rainfall field over time. In the S-PROG set-up for research, three rainfall fields are used to derive the motion vectors. The motion vectors are composed using a pattern-matching algorithm that estimates the displacement between the succeeding input files. A sensitivity analysis by Pulkkinen et al., (2019) showed a limited sensitivity of motion field methods on the nowcasting skill. In this study, the Lucas-Kanade method (Lucas & Kanade, 1981) is applied, this is in line with the study of Imhoff et al., (2020). After the composition of the motion vectors, semi-Lagrangian advection is used to extrapolate the rainfall fields.

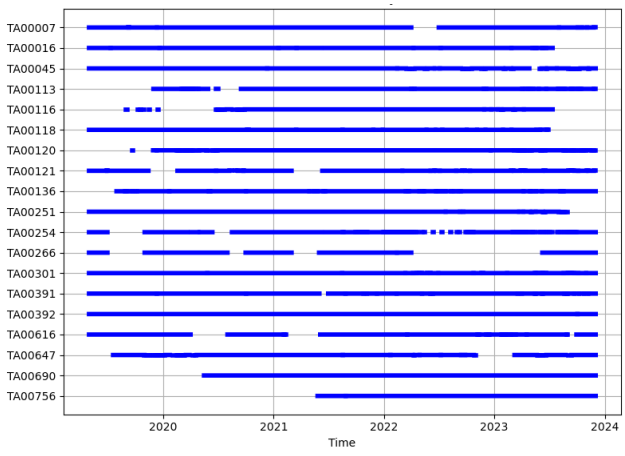


*Figure 2 Data availability of TAHMO observations per station*

The following step in the Pysteps workflow is spectral decomposition. Precipitation behavior depends on its spatial scale (Germann & Zawadzki, 2002). To capture this phenomenon, the precipitation field is divided into six different cascades of spatial scales. This scale decomposition uses Gaussian weight functions on the Fast Fourier Transform (FFT) spectrum. Figure 3 shows an example of the various cascade decomposition levels. Next, the temporal evolution of precipitation is captured using auto-regressive (AR) model parameters per cascade. The AR models capture the temporal dependencies between successive levels and aim to represent evolving rainfall patterns over time. After the AR models are used to predict the future state of each cascade level, the results are to produce a nowcasted precipitation field. This final nowcast result becomes smoother over time. Figure 4 shows an example nowcast for the spatial extent of Ghana. In this figure, the smoothing effect over time is visible. This study uses the default S-PROG parameters as described by Seed, (2003) and Pulkkinen et al., (2019).

### 2.4. Precipitation detection capabilities of the MSG-CPP retrieval products in Ghana

For the first research objective, the capabilities of the MSG-CPP algorithm to detect precipitation and specifically peak precipitation intensities are analyzed for Ghana. In the scope of this research, peak precipitation is defined as the 95% percentile precipitation intensity as measured by the 19 TAHMO stations. To examine the precipitation detection capabilities of the MSG-CPP retrieval products, the MSG-CPP data is compared with TAHMO ground measurements. For all 19 TAHMO station locations the matching pixel in the MSG-CPP retrieval data is determined. The precipitation intensity value of the associated pixel is extracted for the visual as well as the infrared (IR) retrieval algorithm over the complete available time series of the MSG-CPP data. To compare peak precipitation thresholds, the 90% and 95% percentile precipitation is derived over all timesteps with a precipitation intensity > 0.1 mm/h per timestep. This is done for the TAHMO as well as the MSG-CPP IR and visual data, see table 3.

As peak definition the 95% percentile intensity of the TAHMO data is used. However, to examine the peak detection capabilities, the choice is made to compare the 95% percentile TAHMO threshold with the 90% percentile MSG-CPP thresholds. This study aims to examine whether the MSG-CPP retrieval products can detect high precipitation intensities. Expanding the acceptance margin contributes to the overall evaluation of the retrieval products in this context. The daily temporal resolution is added to the analyses to research the effect of temporal

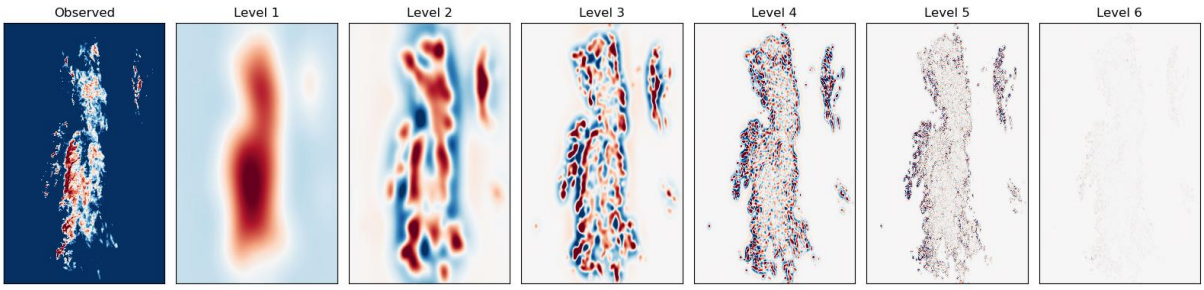


*Figure 3 Example of spatial decomposition into cascades as used in the S-PROG method, adapted from Pysteps tutorial, cascade decomposition*

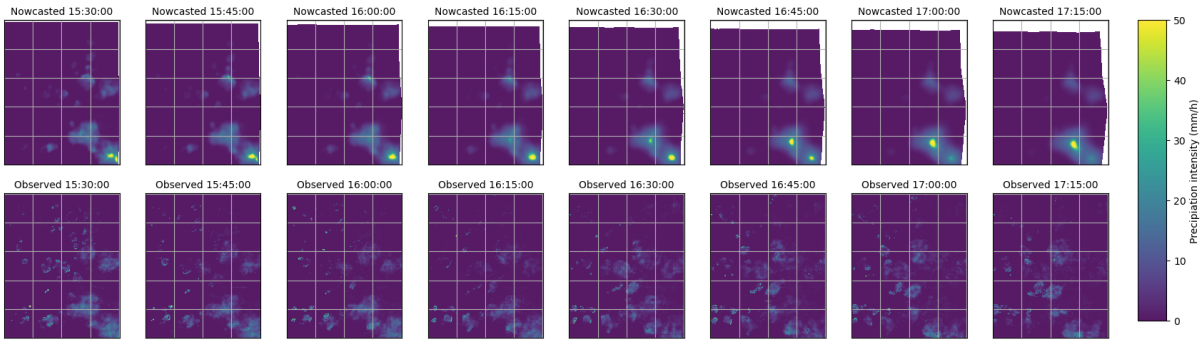


*Figure 4 S-PROG nowcasting example using MSG-CPP IR input data for the spatial extent of Ghana 10/05/2020*

resolution on the detection capabilities, the associated thresholds are presented in table 3.

***Table 3 Precipitation thresholds using the 90% and 95% percentile of precipitating timesteps***

| | **15-min precipitation intensity >0.1 mm/h** | **Daily precipitation >0.1 mm daily** |
|---|---|---|
| TAHMO | | |
| 90% percentile | 3.8 mm/h | 4.7 mm |
| 95% percentile | 7.0 mm/h | 8.1 mm |
| MSG-CPP IR | | |
| 90% percentile | 7.9 mm/h | 16.8 mm |
| 95% percentile | 11.9 mm/h | 29.6 mm |
| MSG-CPP visual | | |
| 90% percentile | 17.9 mm/h | 30.3 mm |
| 95% percentile | 32.5 mm/h | 54.1 mm |

In the detection analyses, the following questions are addressed. Firstly, how well can the MSG-CPP retrieval algorithms detect observed precipitation? Secondly, when TAHMO shows a peak precipitation intensity how often does the MSG-CPP data detect peak intensity as well? And lastly, how often does the MSG-CPP data show a peak intensity which is not observed in the TAHMO measurements? To answer these questions the selected peak events as defined by the thresholds in table 3 are analyzed using a scatterplot and a histogram. Moreover, the Probability Of Detection (POD), the False Alarm Ratio (FAR), and the Critical Succes Index (CSI) are derived as performance indicators, see equations 1 till 3. In these equations, "hits" refers to a timestep where the MSG-CPP rainfall retrieval detected rainfall which was also detected by the TAHMO observations. "Misses" refers to the timesteps in which the TAHMO data shows a precipitation measurement that is not detected by the MSG-CPP algorithm. Finally, "false alarm" represents the timesteps in which the MSG-CPP data detected rainfall and the TAHMO data did not. For the POD and CSI, 1 indicates a perfect score, and 0 is the worst score. For the FAR, 0 is a perfect score and 1 indicates the worst outcome.

$$POD = \frac{hits}{hits + misses} \qquad \text{(equation 1)}$$

$$FAR = \frac{false\ alarms}{false\ alarms\ + hits} \qquad \text{(equation 2)}$$

$$CSI = \frac{hits}{hits + misses + false\ alarms} \qquad \text{(equation 3)}$$

## 2.5. Comparative analysis of satellite-based precipitation data for peak events Odaw catchment

For the second research objective, the precipitation intensity of various satellite-based retrieval products is compared for a selection of peak events. For early warning purposes, the spatial scale of a basin is most applicable in practice. Consequently, the choice is made to select a basin and analyze the difference in precipitation representation for eight heavy precipitation events in this basin. In this analysis the precipitation retrieval products, as presented in section 2.1, are included. For these events, the precipitation intensity on the smallest available timestep and the cumulative rainfall depth are compared. Moreover, the percentual difference in daily rainfall depth is compared to the TAHMO measurements. All precipitation retrieval data is available in pixel format which eases the composition of an average precipitation intensity. To convert the point measurements of the TAHMO data into a precipitation field, Thiessen polygons are applied. In figure 5 the boundaries of the Thiessen polygons are visualized.

***Basin selection***

To select a case-study area, the availability of TAHMO stations is used as the main selection criteria. This led to the selection of the Odaw basin in the Accra region as a case-study area. For this basin there is data available of three nearby TAHMO stations, see figure 5. The Odaw basin has a surface area of 285 km$^2$ and is highly urbanized. The area is subject to frequent flooding, which has large social-economic consequences (Ntajal et al., 2022). A report, published by the Ministry of Works and Housing, states that the average annual rainfall in the basin is 730 mm (Larmie Seth, 2019). For the analyses of the precipitation data, the pragmatic choice is made to derive a square extent around the basin shape. Making clips within the extent of a pixel is computationally complex and for the aim of this analysis, it is not considered of significant influence that the exact basin contours are followed.

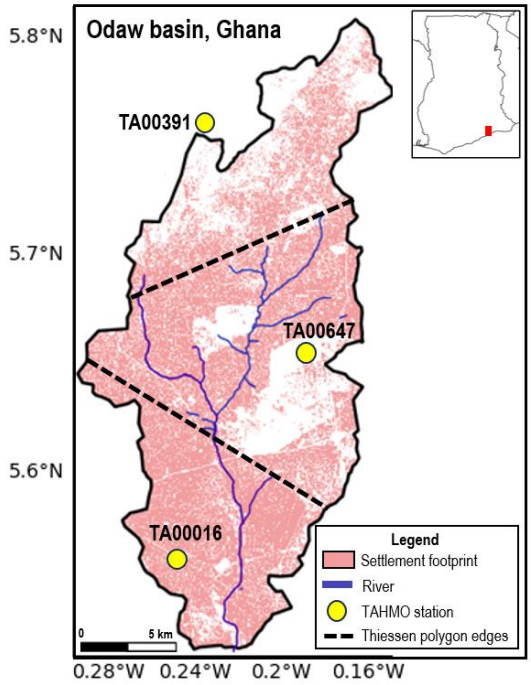


*Figure 5 Odaw Basin study area with TAHMO stations and Thiessen polygons*

***Heavy precipitation event selection for Odaw basin***

To compose a selection of heavy precipitation events for the Odaw catchment, the TAHMO data is used. Firstly, all timesteps that have a NaN value for one of the three TAHMO stations in the Odaw region are removed from the time series. Next, the remaining TAHMO data is resampled to 3-hour and daily precipitation intensities. Of these resampled precipitation intensities, the highest peak events are selected and checked for MSG-CPP, IMERG, and CMORPH data availability. The eight resulting precipitation events are presented in table 4.

*Table 4 Selected heavy precipitation events for Odaw basin*

| Precipitation days | Peak intensity time step in TAHMO observation data (local time) | The period used for nowcasting |
|---|---|---|
| 2020-04-26 | 9:30 | 6:00-10:30 |
| 2020-05-10 | 17:00 | 13:30-18:00 |
| 2020-05-28 | 16:45 | 13:00-17:30 |
| 2020-10-10 | 9:15 | 5:30-10:00 |
| 2022-05-06 | 16:30 | 13:00-17:30 |
| 2022-05-21 | 20:30 | 17:00-21:30 |
| 2023-03-07 | 3:45 | 01:30-6:00 |
| 2023-04-27 | 17:00 | 14:30-18:00 |

## 2.6. Satellite-based precipitation nowcasting

For the third research objective, the nowcasting skill of the S-PROG method is analyzed for Ghana. For this analysis, the MSG-CPP IR data is used as input data. This dataset is selected because it has the potential to be operationally applied due to its relatively short latency. The MSG-CPP visual algorithm is not used because its daylight dependency is considered impractical for operational purposes. In the performance analysis of the S-PROG method, the nowcasted precipitation fields are compared to the retrieval product itself, as observed at the respective lead times. This approach enables the evaluation of the nowcasting algorithm independently from the evaluation of the retrieval product, which is studied in the first two research objectives.

To get a comprehensive understanding of the S-PROG nowcast characteristics and its overall performance the choice is made to evaluate the satellite-based precipitation nowcast for various spatial extents and scopes. These different evaluation perspectives are shortly stated below and further elaborated in the following paragraphs.

1) Conducting a quantitative nowcast evaluation using the Fraction Skill Score (FSS) for the complete area extent of Ghana with 116 precipitation events > 5.0 mm/h.
2) Reflecting qualitatively on the S-PROG nowcasting characteristics using the Odaw basin area extent and the eight selected heavy precipitation events as presented in table 4
3) Analyzing the effects of different temporal resolutions in the input data on the nowcasting skill of the S-PROG model. This is done quantitatively using the FFS for the area extent of Ghana and subsequently using the Mean Absolute Error (MAE) for the Odaw basin. For the FSS as well as the MAE, 116 precipitation events > 5.0 mm/h are used.
4) Reflecting qualitatively on the S-PROG nowcasting characteristics for the various temporal resolutions in input data. This is done for the Odaw basin and using the eight selected precipitation events as presented in table 4

To analyze skillful lead times of the S-PROG method a large event selection has been made. The 5 mm/h threshold is selected as it represents a significant precipitation event while finding a balance in which sufficient precipitation events were present in the available MSG-CPP IR data. Over the complete MSG-CPP IR time

series, all precipitation events > 5 mm/h in the Odaw basin are selected. This resulted in the selection of 116 events. For these 116 events, a nowcast was composed including the timesteps four hours before the peak precipitation event and half an hour after. In literature, the highest found skillful lead time of the S-PROG nowcasting algorithm is 4 hours (Burton et al., 2022). By selecting a time window of 4.5 hours this lead time is included in the analyses, while limiting the computational demands of the analysis. For the derived time window, a nowcasting loop is composed in which each iteration starts one timestep later in time. For all of the different nowcast evaluation approaches, the nowcast algorithm is applied over the complete area extent of Ghana. To subsequently assess the S-PROG nowcasting patterns in more detail, a focus is given to the eight selected precipitation events in the Odaw basin. For these events, the precipitation intensity per timestep and the cumulative precipitation per event are analyzed.

Additionally, the sensitivity of the S-PROG method to the temporal resolution of input data is explored. In this study, emphasis is given to the MSG-CPP retrieval products as they have the largest potential to be used for operational nowcasting. This assumption is partly based on the fact that the MSG-CPP data has the highest temporal resolution. By examining how the S-PROG method responds to changes in the temporal resolution of input data, it is possible to analyze whether alternative satellite-based retrieval products with lower temporal resolutions would offer possibilities. For this sensitivity analysis, the same 116 precipitation events > 5.0 mm/h are used. However, the MSG-CPP IR data is aggregated into timesteps of 30- and 60-minutes. To compare the nowcasting performance of the various temporal resolutions, the FSS is derived for the complete Ghana extent. Moreover, the Mean Absolute Error (MAE) is composed for the Odaw basin area. Finally, there is again given the focus on the eight heavy precipitation events for the Odaw basin to reflect qualitatively on the nowcast characteristics originating from varying temporal resolutions.

***Nowcasting performance indicators***

To evaluate the nowcasting performances for the complete Ghana area extent the fraction skill score (FSS) is utilized. The FSS, as described by Roberts & Lean, (2008), is selected as a performance indicator because it enables performance evaluation for various spatial scale levels. Evaluation on various scale levels is of value to reflect on the applicability of nowcasting results. Smaller spatial scales are of value to anticipate on localized events. However, nowcast data on large-scale levels can be of value for hydrological models on a basin scale. Equations 4 to 6 are used to quantify the similarity between observed and nowcasted precipitation fields and derive the FSS. The FFS varies from 0, which indicates no skill, to 1, a perfect skill. The nowcast is generally considered skillful when FSS > 0.5 + $\frac{f_0}{2}$ , where $f_0$ is the area of the observed scale divided by the area of the observed domain (Roberts & Lean, 2008). The observed domain refers to the spatial scale level of the evaluation and the associated area of these grid cells. The area of the observed domain is the total area for which the nowcast is composed. In the scope of this study, it refers to the area extent of Ghana. As evaluation scale levels 3, 9, 60, 180, and 300 km are selected. These are all multiples of the spatial resolution of the MSG-CPP IR data of 3 km. For the spatial scales up to 60 km an FSS > 0.5 is considered skillful. For 180 and 300 km these thresholds are respectively 0.54 and 0.60.

$$FSS_{(n)} = 1 - \frac{MSE_{(n)}}{MSE_{(n)ref}} \qquad \text{(Equation 4)}$$

$$MSE_{(n)} = \frac{1}{N_x N_y} \sum_{i=1}^{N_x} \sum_{j=1}^{N_y} \left[O_{(n)i,j} - M_{(n)i,j}\right]^2 \qquad \text{(Equation 5)}$$

$$MSE_{(n)ref} = \frac{1}{N_x N_y} \sum_{i=1}^{N_x} \sum_{j=1}^{N_y} O_{(n)i,j}^2 + \sum_{i=1}^{N_x} \sum_{j=1}^{N_y} M_{(n)i,j}^2 \qquad \text{(Equation 6)}$$

Where:

*$N_x$ = Number of columns in the area extent of n x n cells*

*$N_y$ = Number of rows in the area extent of n x n cells*

*$O_{(n)i,j}$ = Amount of observed grid cells in a specific neighborhood size n that exceed an intensity threshold of 1.0 mm/h*

*$M_{(n)i,j}$= Amount of nowcasted grid cells in a specific neighborhood size n that exceed an intensity threshold of 1.0 mm/h*

*$MSE_{(n)}$= Mean Squared Error between observed and nowcasted values for a specific neighborhood size n*

*$MSE_{(n)ref}$= The largest possible MSE between observations and nowcast values for a specific neighborhood size n*

The FSS mainly evaluates the spatial pattern of the composed nowcast data. To additionally reflect on the nowcasted precipitation intensities, the Mean Absolute Error (MAE) is derived using equation 7. The MAE is derived for the spatial extent of the Odaw basin and the 116 precipitation events in various temporal resolutions.

$$MAE = \frac{\sum_{i=1}^{n} M_i - O_i}{n} \qquad \text{(equation 7)}$$

**Where:**

$M_i$ = *Nowcasted average precipitation intensity in the Odaw basin*

$O_i$ = *Observed average precipitation intensity in the Odaw basin*

$n$= *Amount of included nowcasting timesteps*

# 3. Results

## 3.1. Precipitation detection capabilities of the MSG-CPP retrieval products

### *MSG-CPP IR retrieval*

To analyze the precipitation detection capabilities of the MSG-CPP products first the overall detection of precipitation (>0.1 mm/h) is examined. Subsequently, a focus is given to peak precipitation intensities. In the scope of this study peak precipitation is defined as the precipitation intensity of the 95% percentile TAHMO and 90% percentile MSG-CPP data, see section 2.4. The results presented in this section include the data of all 19 TAHMO stations and their associated pixel value in the MSG-CPP data. Figure 6 shows scatterplots and histograms of the TAHMO and MSG-CPP IR peak precipitation data based on percentile thresholds as

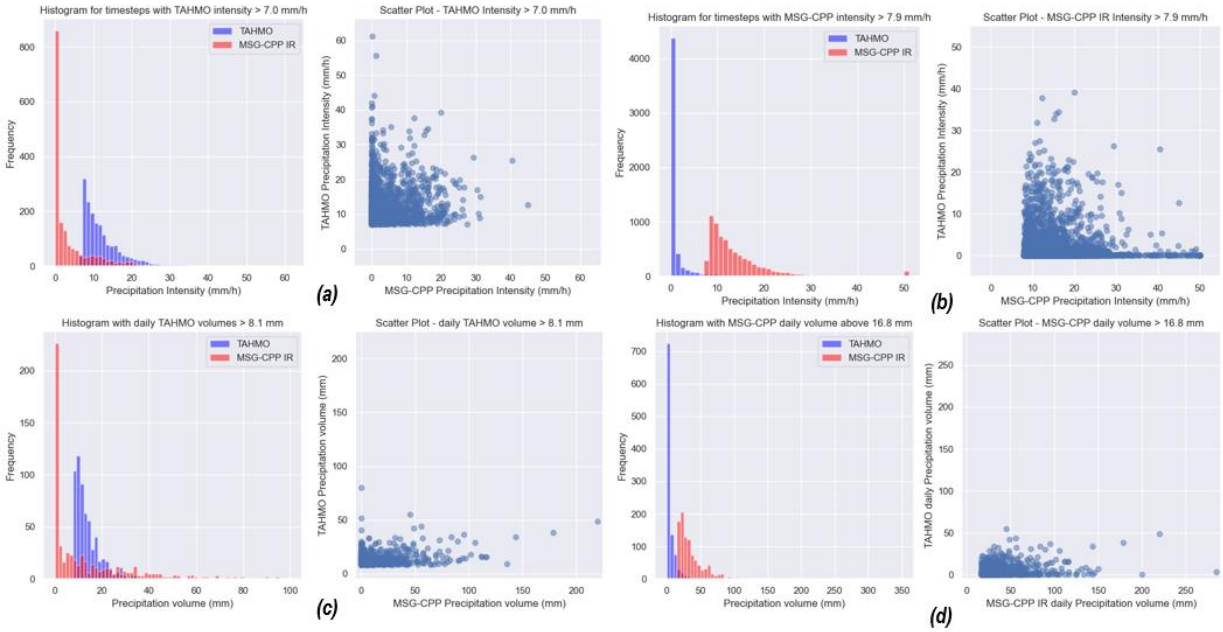


***Figure 6 Histograms and scatterplots showing the peak precipitation events in the TAHMO and MSG-CPP IR data. (a) and (b) present a temporal resolution of 15 minutes, (c) and (d) a daily temporal scale.***

***Table 5 Performance indicators precipitation detection MSG-CPP IR retrieval product using TAHMO measurements of 19 stations in Ghana***

| TAHMO threshold | MSG-CPP IR threshold | Number of events | POD<br>1 = perfect score<br>0 = worst score | FAR<br>0 = perfect score<br>1 = worst score | CSI<br>1 = perfect score<br>0 = worst score |
|---|---|---|---|---|---|
| **15-minute timesteps** | | | | | |
| >0.1 mm/h | >0.1 mm/h | 169648 | 0.49 | 0.75 | 0.20 |
| >7.0 mm/h | >0.1 mm/h | 135818 | 0.69 | 0.98 | 0.02 |
| >7.0 mm/h | >7.9 mm/h | 15990 | 0.19 | 0.95 | 0.04 |
| **Daily timesteps** | | | | | |
| >0.1 mm | >0.1 mm | 10290 | 0.55 | 0.53 | 0.34 |
| >8.1 mm | >0.1 mm | 7606 | 0.68 | 0.94 | 0.05 |
| >8.1 mm | >16.8 mm | 1420 | 0.31 | 0.81 | 0.13 |

presented in table 3. Figure 6 (a) and (c) show the timesteps selection after applying the TAHMO peak threshold, additionally (b) and (d) show the timesteps when applying the MSG-CPP IR peak thresholds. In table 5 the Probability Of Detection (POD), the False Alarm Ratio (FAR), and Critical Succes Index (CSI) are shown. Already in the definition of the thresholds, it is noticeable that there is a difference in precipitation intensities. The derived MSG-CPP IR percentile thresholds are significantly higher than the TAHMO percentiles. Besides the differences in intensity threshold, the scatterplots show that a clear correlation between the MSG-CPP IR retrieval product and the TAHMO measurements is lacking.

In the first row of table 5, the overall capability of detecting precipitation is shown, this led to a POD of 0.49. The high false alarm ratio of 0.75 shows that the MSG-CPP algorithm often detects precipitation, while the TAHMO ground measurement stations do not observe any rainfall. For peak observations in the TAHMO data, the POD becomes higher, however, the FAR also increases which leads to an overall lower CSI. When solely looking at peak observations for the TAHMO as well as the MSG-CPP IR data, the POD is 0.19. Besides the differences in precipitation intensities, the histograms show that the MSG-CPP IR data has a larger intensity spread compared to the TAHMO stations. The histogram of the MSG-CPP IR-based peaks barely shows any overlap with the TAHMO distribution. Moreover, it seems that the MSG-CPP IR algorithm has a maximum precipitation intensity of 50 mm/h (for a 15-minute timestep). To examine the impact of the temporal resolution on precipitation detection, a similar peak comparison is executed using daily timesteps. On a daily temporal resolution, the MSG-

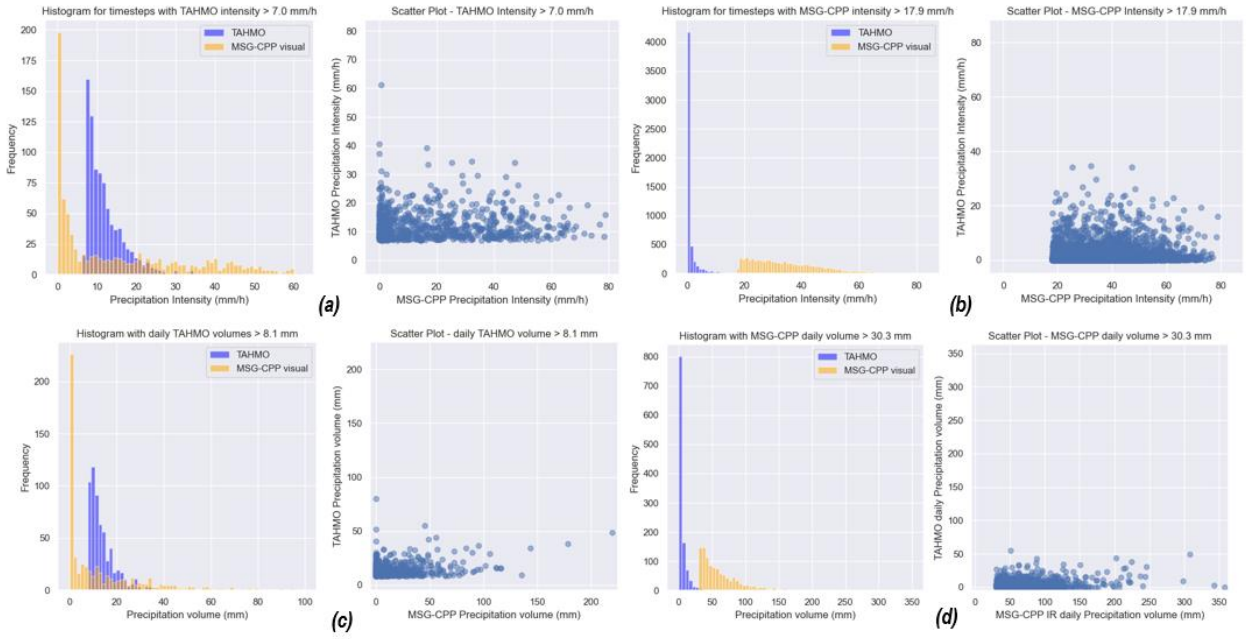


***Figure 7 Histograms and scatterplots showing the peak precipitation events in the MSG-CPP visual and TAHMO data. (a) and (b) present a temporal resolution of 15 minutes, (c) and (d) a daily temporal scale***

***Table 6 Performance indicators precipitation detection MSG-CPP visual retrieval product using TAHMO measurements of 19 stations in Ghana***

| **TAHMO threshold** | **MSG-CPP visual threshold** | **Number of events** | **POD** 1 = perfect score 0 = worst score | **FAR** 0 = perfect score 1 = worst score | **CSI** 1 = perfect score 0 = worst score |
|---|---|---|---|---|---|
| **15-minute timesteps** | | | | | |
| >0.1 mm/h | >0.1 mm/h | 139228 | 0.81 | 0.80 | 0.19 |
| >7.0 mm/h | >0.1 mm/h | 133030 | 0.94 | 0.99 | 0.01 |
| >7.0 mm/h | >17.9 mm/h | 14164 | 0.39 | 0.95 | 0.05 |
| **Daily timesteps** | | | | | |
| >0.1 mm | >0.1 mm | 10701 | 0.58 | 0.55 | 0.34 |
| >8.1 mm | >0.1 mm | 8244 | 0.64 | 0.95 | 0.05 |
| >8.1mm | >30.3 mm | 1522 | 0.31 | 0.83 | 0.12 |

CPP IR peak threshold is approximately twice the TAHMO peak threshold. Additionally, the results show a reduction in the FAR and an increase in POD. This has a positive effect on the CSI. These results show that the MSG-CPP detection capabilities are sensitive to its temporal resolution.

***MSG-CPP Visual retrieval product***

Figure 7 shows scatterplots and histograms of the peak intensity timesteps of the MSG-CPP visual retrieval product and the TAHMO measurements. Figure 7 (a) and (c) show the timesteps selection after applying the TAHMO peak thresholds, additionally (b) and (d) show the timesteps when applying the MSG-CPP visual peak thresholds. In table 6 the POD, FAR, and CSI are presented for the various precipitation intensity thresholds as defined in Section 2.4. The number of selected peak events is reduced compared to the IR-based time series due to the decreased number of available timesteps in the data (only day times). As a first observation, it is visible that the peak percentile thresholds of the MSG-CPP visual data are almost 5 times higher than for the TAHMO data, and more than double the MSG-CPP IR threshold. These are clear indicators that the precipitation intensities in the MSG-CPP visual retrieval algorithm are significantly overestimated. Moreover, the associated scatterplots of the peak timesteps lack a clear correlation. In the histograms, it is visible that many timesteps indicate a peak intensity in one of the datasets while the other does not present any precipitation occurrence. Additionally, the MSG-CPP visual data has a much larger spread in peak precipitation intensities compared to the TAHMO observations.

The POD for detecting precipitation is 0.81, this is significantly higher than for the IR retrieval product. However, the FAR ratio of 0.80 is also higher, which leads to similar a CSI index. For TAHMO peak timesteps the POD is even 0.94, but the associated FAR is 0.99. For detecting peak precipitation intensities in both the TAHMO and MSG-CPP visual data, the POD is 0.39, also this is higher compared to the IR dataset. Interesting is that on a daily temporal scale the POD as well as the FAR decrease. These have the opposite effect on the CSI. Nevertheless, the overall CSI improves for a daily temporal resolution compared to the 15-minute analyses. On a daily resolution, the performance indicators of the MSG-CPP IR and visual data are comparable.

## 3.2. Comparative analysis of satellite-based precipitation products for peak events in the Odaw catchment

To compare the different datasets, a visual representation of the eight selected peak events, as presented in table 4, is made. This is done for the complete extent of Ghana. Figure 8 shows the precipitation maps for the peak event on 28 May 2020, the visualizations of the other events are presented in Appendix A. In these figures, it is visible that the overall patterns in the precipitation retrievals have clear similarities. Due to the limited coverage of the TAHMO stations, it is challenging to compare the retrieval products with patterns in TAHMO measurements. However, from the first interpretation, it seems that the retrieval products frequently show precipitation coverage, which is not detected by the TAHMO stations. This is for example visible for the 10th and 28th of May 2020. On the other hand, on the 6th of May 2022, the TAHMO station in the Accra region showed a clear precipitation peak, which is not recognizable in any of the retrieval products.

Moreover, it is visible that the MSG-CPP visual product shows higher precipitation intensities than all the other retrieval products. Also, the difference between the IMERG Early and Final products is clearly recognizable, especially in the spatial extent of the precipitation field, for example, the 10th of May 2020 event. Another remarkable observation is that on the 6th of April 2020, the MSG-CPP visual algorithm detected a large precipitating field in the Northeast of the county which is not at all visible in the MSG-CPP IR retrieval product.

To compare the retrieval products more quantitatively, a focus is given to the Odaw basin area. In figure 9 the cumulative precipitation of the eight selected heavy precipitation events is presented. More detailed precipitation intensity graphs per dataset can be found in Appendix B. Important to note is that the graph representing the MSG-CPP visual algorithm is interrupted when the data availability ends (periods of the day without daylight). This limits the possibility of analyzing the rainfall intensities of the MSG-CPP visual product for all peak events. Still, it is visible that the MSG-CPP visual product extremely overestimates the precipitation intensity compared to the TAHMO measurements. This observation is in line with the observations in section 3.1. Besides the overestimation of the MSG-CPP visual product, several other observations can be made. Firstly, for almost all events, the satellite products overestimate the

precipitation intensity in relation to the TAHMO observations. This could be due to the limited product calibration using ground data in the Ghana region. Another possibility is that the point measurement stations in the TAHMO data are not suffieciently able to represent peak events and consequently underestimate the precipitation depth. A next observation is that overall, the IMERG Early, IMERG Final, CMORPH and MSG-CPP retrieval products show comparable shapes in their cumulative precipitation graphs for the selected events. Despite the differences in cumulative precipitation depth, the start time, end time, and time of peak precipitation vary in the order of magnitude of one to two hours.

To assess which of the satellite-based retrieval products most closely corresponds with the TAHMO measurements, the percentual difference in daily precipitation depth is compared with TAHMO data, see figure 10. Again, a clear overestimation of the MSG-CPP visual data is visible. All other precipitation products show overestimations up to 500%. Only the MSG-CPP IR data also shows two underestimations of the measured precipitation depth. Moreover, the MSG-CPP IR data has a slightly larger spread in % differences compared to the IMERG and CMORPH data. Additionally, it is visible that the 27 April 2023 event has the lowest % difference for most datasets. This peak event has in comparison to the other selected peak events a lower cumulative precipitation depth. Potentially, lower precipitation peaks are easier to detect using satellite-based precipitation products than higher peak events. This hypothesis is further discussed in the discussion section.

Based on the analyses of these eight heavy precipitation events in the Odaw basin, it cannot be concluded which of the satellite products is best at representing peak events. However, you could expect that the precipitation products with a larger latency (CMORPH and IMERG final) would show a higher correspondence with measurement data due to their increased usage of data sources and postprocessing steps. However, this hypothesis cannot be substantiated based on the presented results. The IMERG Early and the MSG-CPP IR retrieval product, both with low latencies, show similar abilities in representing peak precipitation timing and depth as IMERG Final and CMORPH. The implications that this observation has in the face of nowcasting using satellite-based retrieval products are also addressed in the discussion section.

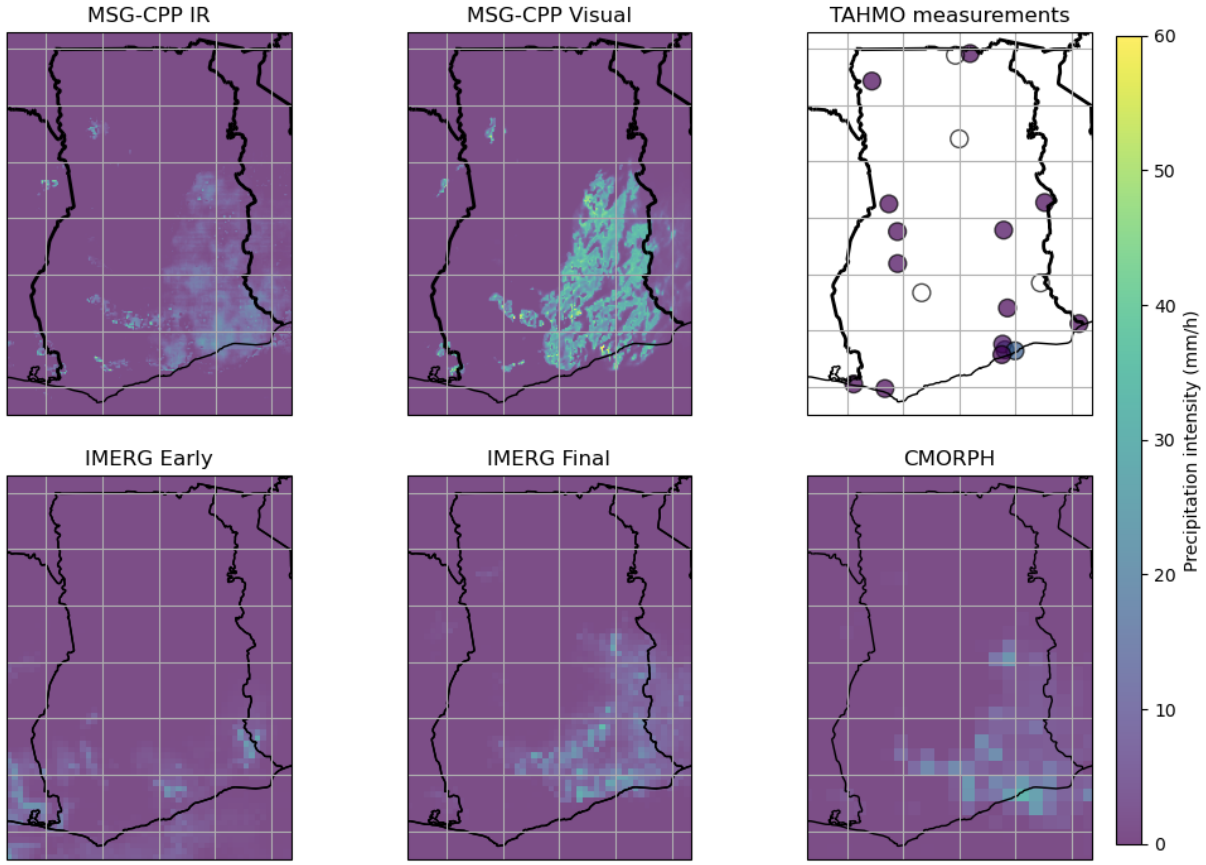


***Figure 8 Precipitation retrieval products representing precipitation intensity on 28/05/2020, 16:30***

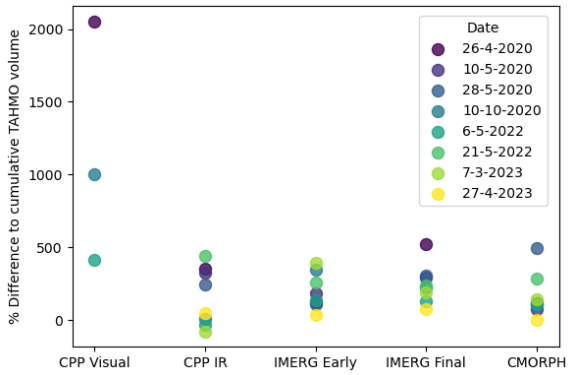


***Figure 10 Percentual (%) difference between cumulative precipitation depth for retrieval products and TAHMO observations***

### 3.3. Satellite-based precipitation nowcasting

Based on the results of the previous sections, questions can be raised concerning the applicability of the MSG-CPP retrieval products for nowcasting due to their limited correspondence with TAHMO measurements. The results in this section aim to reflect on the nowcasting potential of the S-PROG method given the spatial and temporal resolution of satellite-based retrieval products. The propagation of uncertainties that originate from the quality of the retrieval products is not incorporated in the presented results. When examining the nowcasting skill, the nowcast data is compared with the observed satellite image on its given lead time. In this nowcast analysis, a focus is given to the MSG-CPP IR retrieval product. This product is selected because it has the smallest latency and highest temporal and spatial resolution. The MSG-CPP visual product is due to its daylight dependence impractical.

First, the nowcasting skill of the S-PROG method is analyzed for a variety of lead times and spatial scale levels for the complete area extent of Ghana. This is done using 116 observed precipitation events >5.0 mm/h for a timestep of 15 minutes. Next, the nowcast results of the eight selected peak events are discussed to observe the nowcasting patterns in more detail. For the eight heavy precipitation events the nowcast algorithm is applied for the complete area extent of Ghana, however, the results are specifically analyzed for the Odaw basin. Additionally, the sensitivity of the S-PROG method to various temporal resolutions in input data is analyzed. This is again done for the complete Ghana area extent and the 116 precipitation events.

***Quantitative assessment of skillful lead times of S-PROG nowcast model in Ghana***

The S-PROG nowcast method is applied for 116 precipitation events in Ghana. Figure 11 shows boxplots of the FSS performance indicator per lead time and spatial scale. The spatial scale component is included to evaluate

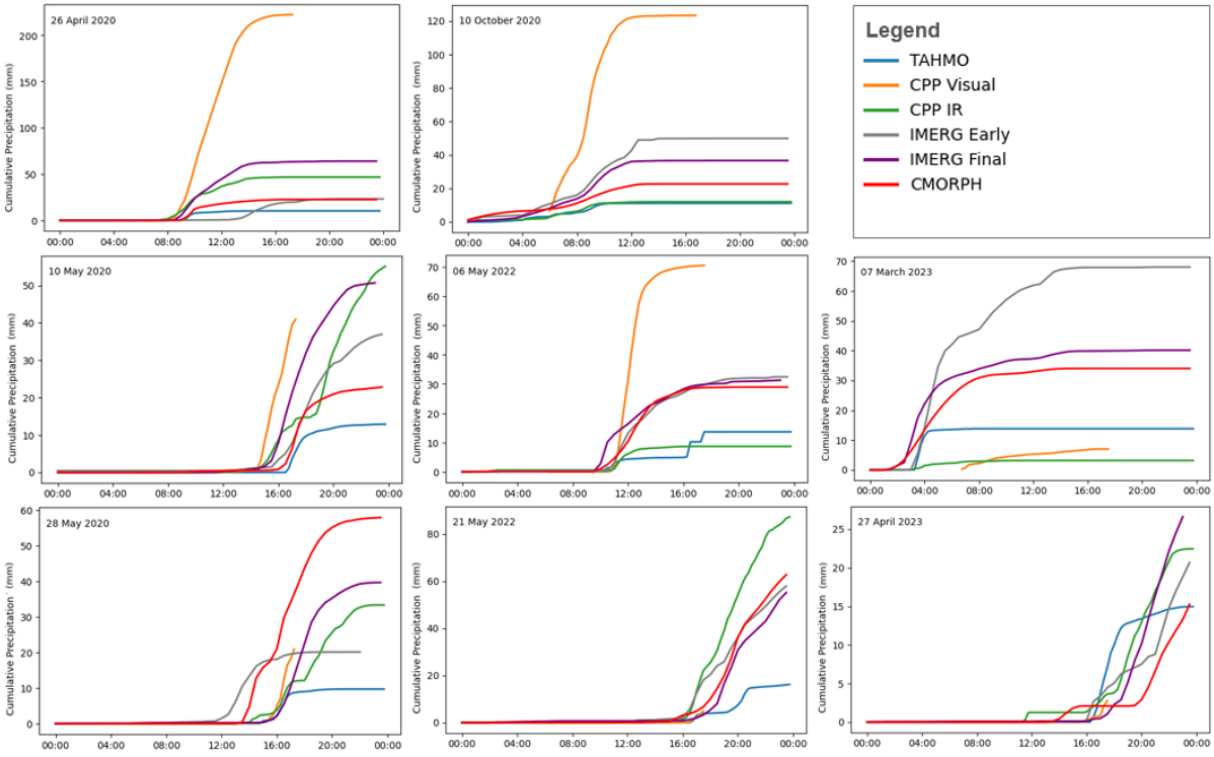


***Figure 9 Cumulative precipitation of various retrieval products and TAHMO observations for the eight selected heavy precipitation events***

on the applicability of the nowcast results for various spatial extents. Important to consider is that the latency of the MSG-CPP retrieval data is not included in the presented lead time. From a practical perspective, the lead times starting from 45 min latency could be used in operational nowcasting. In the plot, the dotted lines indicate the FSS threshold for skillful performances, as discussed in Section 2.6. Based on the presented results, the following observations are made. Firstly, the variation in FSS per spatial scale and lead time is significant. This shows a large variance in nowcasting performance per event and is an indication that some precipitation patterns can be nowcasted with more accuracy than others. Moreover, the nowcasting results show a decreasing performance with increasing lead times and higher performances for large spatial scale levels. These observations are in line with many other nowcasting studies, such as van der Kooij, (2021) and Imhoff et al., (2020). Additionally, it is visible that the spread in derived FSS increases with the lead time. This indicates that the certainty of the nowcast performance decreases with the lead time.

In table 7 the maximum skillful lead times are presented by using the median and the 75% percentile results. Due to the large spread in FSS scores, the skillful lead time differs significantly between the two columns. Taking into consideration the 45-minute latency of the MSG-CPP IR data, the median nowcast results with a spatial scale of 60, 180, and 300 km show nowcast results that could be operationally applicable. Skillful results on these scale levels can be of value for hydrological models on a basin scale.

*Table 7 Maximum skillful lead time of S-PROG nowcast in Ghana for various spatial scale levels*

| Spatial scale level FSS score | Maximum skillful lead time of median | Maximum skillful lead time of 75% percentile |
|---|---|---|
| 3 km | 30 min | 0 min |
| 9 km | 45 min | 15 min |
| 60 km | 90 min | 45 min |
| 180 km | 120 min | 60 min |
| 300 km | 135 min | 60 min |

### *S-PROG nowcasting characteristics in the Odaw basin for eight selected events*

To get a better understanding of the S-PROG nowcasting behavior, the nowcast results of the eight selected precipitation events as presented in table 4 are analyzed in more detail for the Odaw basin. Appendix C shows per event the observed and nowcasted precipitation intensities throughout the time. In this section, specific graphs are featured to substantiate the analyses of the results. A first observation is that the correspondence between the nowcast and the observed precipitation highly varies per event and the nowcasting start time. For example, the nowcasts of 26 April 2020 show significant correspondence with the observed data, already 2.5 hours before the peak intensity, see figure 12. For some of the other events the nowcast is not at all capable of detecting the upcoming precipitation wave, for example, 27th April 2023 in figure 12. In Appendix A, a visualization is given of the precipitation fields of the eight precipitation events. For the 26th of April 2020, a large dense precipitation field is visible. The S-PROG method shows high skill in nowcasting such precipitation patterns. On the other side, the precipitation event on the 27th of April 2023 has a more scattered and irregular precipitation pattern. These patterns are harder to capture by the S-PROG nowcast

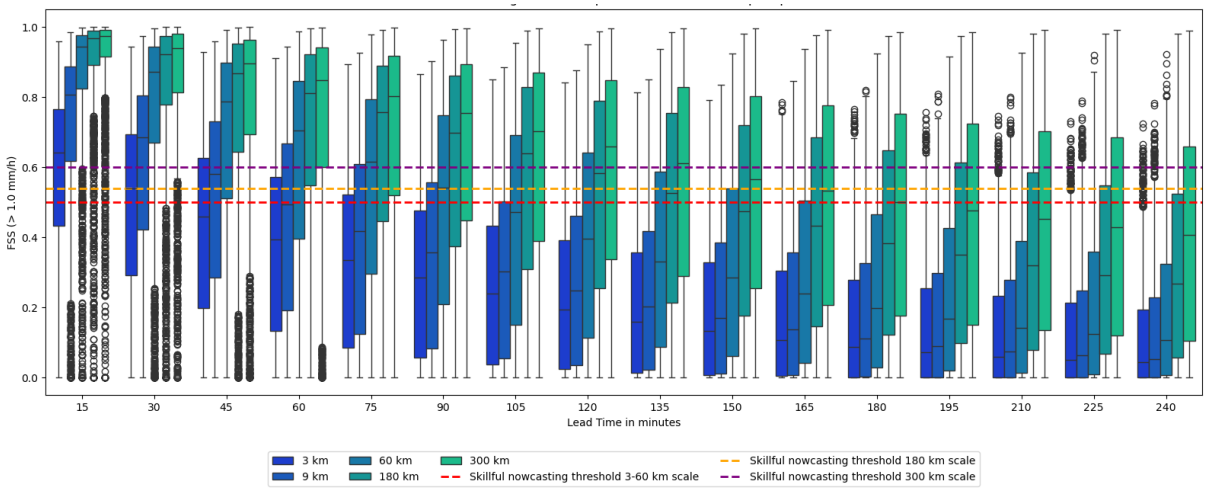


*Figure 11 Fraction Skill Score (FFS) of S-PROG nowcast in Ghana using 116 precipitation events and MSG-CPP IR retrieval product*

method. In the graph, it is visible that the nowcast completely misses the precipitation for the Odaw basin.

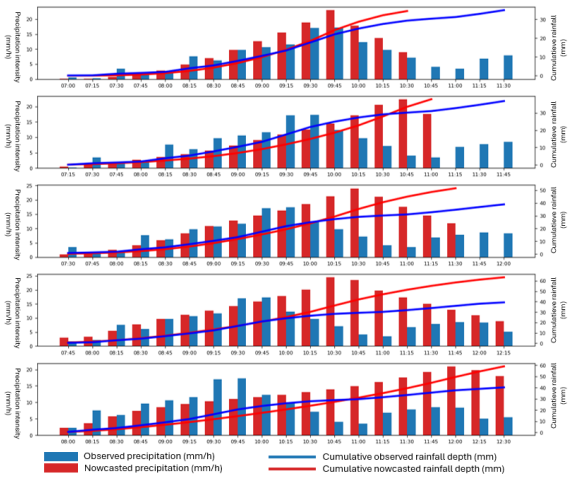


***Figure 12 Observed and nowcasted precipitation for the Odaw basin 26/04/2020***

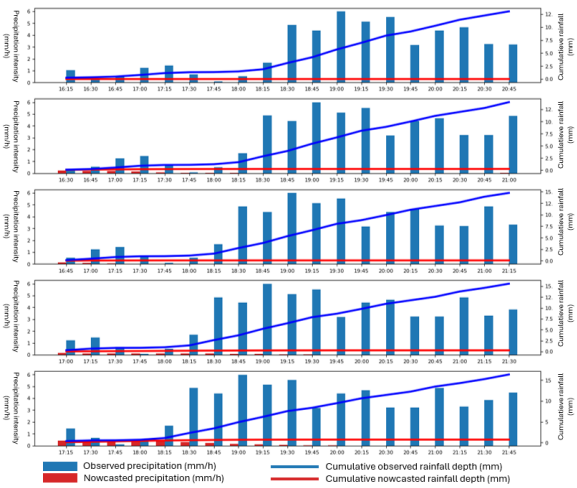


***Figure 13 Observed and nowcasted precipitation for the Odaw basin 27/04/2023***

An additional observation is that the S-PROG method has difficulties representing precipitation with varying intensities. The nowcast results show the tendency to produce one precipitation wave. The increasing or decreasing precipitation patterns in the input data are extrapolated in the nowcast. Consequently, the cumulative precipitation depth can approximate the observed rainfall depths, however, the intensity distribution over time is not well captured. Examples of this phenomenon are presented in figures 14 and 15.

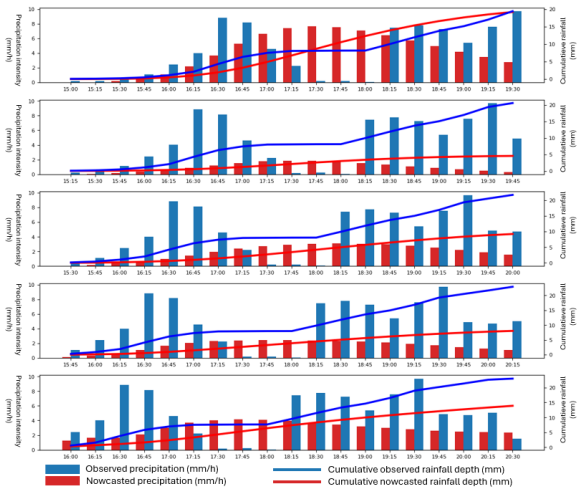


***Figure 14 Observed and nowcasted precipitation for the Odaw basin 28/05/2020***

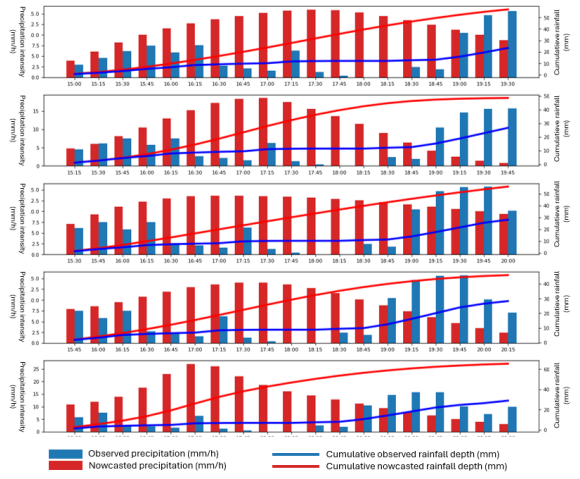


***Figure 15 Observed and nowcasted precipitation for the Odaw basin 10/05/2020***

### *S-PROG sensitivity to the temporal resolution of input files*

Various input data attributes potentially influence the nowcasting performances of the S-PROG model. Partly due to its high temporal resolution, this study emphasized the potential of the MSG-CPP retrieval product. To the best of our knowledge, it is currently the only satellite-based retrieval product in the public domain that is available on this temporal resolution. However, as discussed in sections 3.1 and 3.2, the correspondence between the MSG-CPP products and TAHMO observations in Ghana is limited. Potentially there are other, lower temporal resolution products, which better represent precipitation in Ghana. Consequently, this raises the question of how sensitive the S-PROG nowcasting method is to the temporal resolution of its input data. The results in this section show the S-PROG nowcasting performances using the MSG-CPP IR data with an aggregated temporal resolution of 30- and 60

minutes. For this evaluation, the same 116 precipitation events are used as for the boxplot in figure 11.

The boxplots in figure 16 and figure 17 show the FSS results of the S-PROG nowcast with the 30- and 60-minute temporal resolution in input data. The FSS performance patterns as a function of lead time and spatial scale are similar to in the 15-minute nowcast results in figure 11. When visually comparing the boxplots, a decreasing skill is observed for lower temporal resolutions. However, at first sight the sensitivity to temporal resolution seems limited. In table 8, the maximum skillful lead times of the median and 75% percentile are presented per spatial scale and temporal resolution. While the boxplot differences seem limited at first, the effect on the skillful lead time definition is significant, especially for the 75% percentile definition.

To examine how the temporal resolution of the input data impacts the accuracy of the precipitation estimates, the MAE is derived between the nowcasted and observed precipitation data for the Odaw basin, see figure 18. For this MAE the same 116 events are used as presented in the boxplots. It is visible that the MAE reduces with a decreasing temporal resolution. This indicates that the nowcast results have a higher accuracy in estimating precipitation intensities when a lower resolution of input data is used. This is remarkable because the FSS performance indicator showed a decreasing performance with lower temporal resolutions.

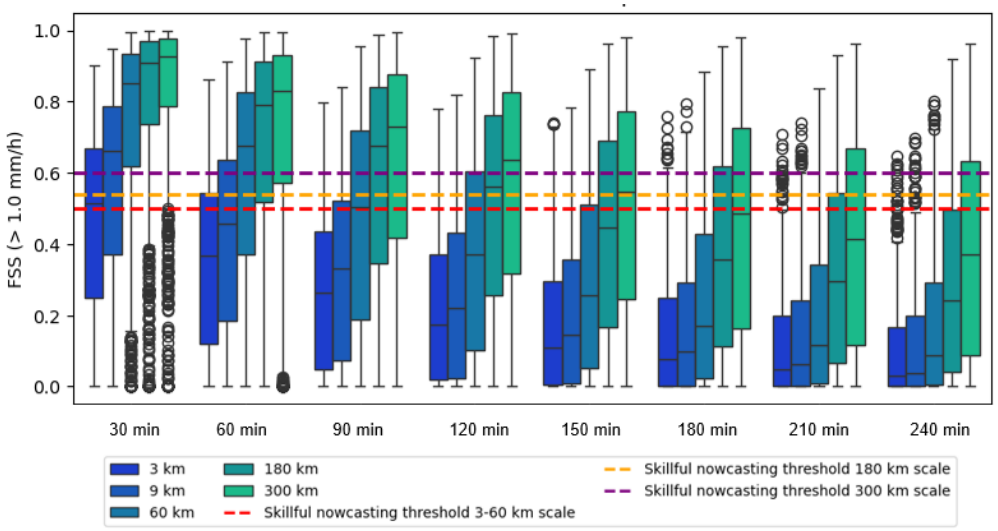


*Figure 16 FFS of S-PROG nowcast in Ghana using 116 precipitation events and 30 min aggregated MSG-CPP IR input data*

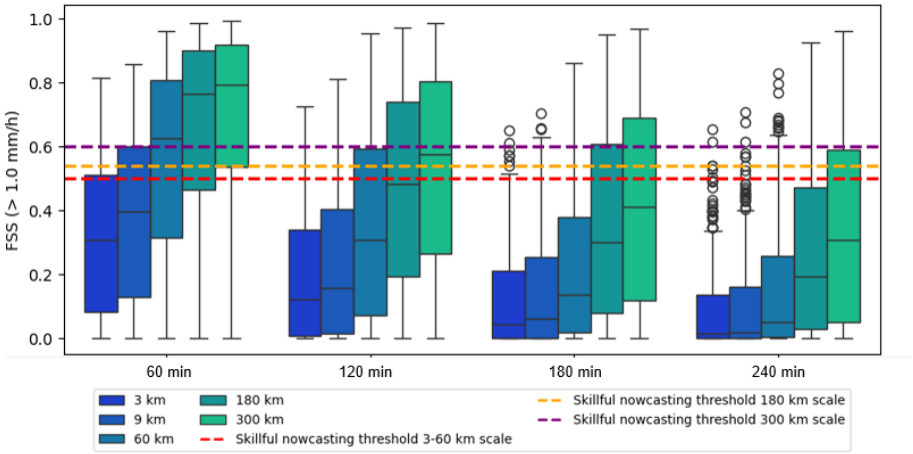


*Figure 17 FFS of S-PROG nowcast in Ghana using 116 precipitation events and 60 min aggregated MSG-CPP IR input data*

To assess in more detail the cause of a reducing MAE with lower temporal resolutions, a nowcast for the Odaw basin is made for the eight heavy precipitation events as presented in table 4. These results are presented in Appendix C, in this paragraph some graphs originating from these figures are included. Overall, the results of the 30- and 60-minute nowcasting graphs show similar nowcasting performance patterns as the 15-minute data. The growth and decay of precipitation are often extrapolated, and this causes differences in observed and nowcasted precipitation intensities. This phenomenon is, for example, clearly visible for the 10th of May 2020 in figure 19. In the 7:15 AM nowcast, the observed peak precipitation wave is missed. When the increase in precipitation is captured by the nowcast input files of later iterations, the increase in precipitation intensity is extrapolated. Subsequently, the decay of the precipitation wave is not well captured which leads to overestimations in rainfall intensities. However, it seems that for the 30- and 60-minute timestep this extrapolation is less extreme compared to the 15-minute data. This is also noticeable in the nowcasts for the 21st of May 2022 and the 26th of April 2020 in figure 20 and figure 21. If precipitation intensities show reduced overestimations of nowcasted precipitation, this could explain the lower MAE for lower temporal resolutions.

A hypothesis concerning the cause of these reduced extrapolation patterns is as follows. The 15- 30- and 60-minute nowcasts all use three input files to determine their advection field. However, these are the three most recent input files before the nowcast start time. For example, when aiming to compose a nowcast at 13:00, the 15-minute dataset uses the input files of 12:15, 12:30, and 12:45. However the 30-minute dataset uses 11:30, 12:00, 12:30, and the 60-minute nowcasts uses 10:00, 11:00 and 12:00. The lower temporal resolution potentially captures the high variability in precipitation less well, which led to a lower FSS. However, the reduction of extremes in precipitation extrapolation results in a lower overall MAE. Additionally, the larger timeframe of the lower resolution nowcasts has the potential to track the movement of a cloud over a longer period. This potentially increases the quality of velocity estimations. It could explain why the 60-minute nowcast on the 27th of April 2023 at 17:15 captures

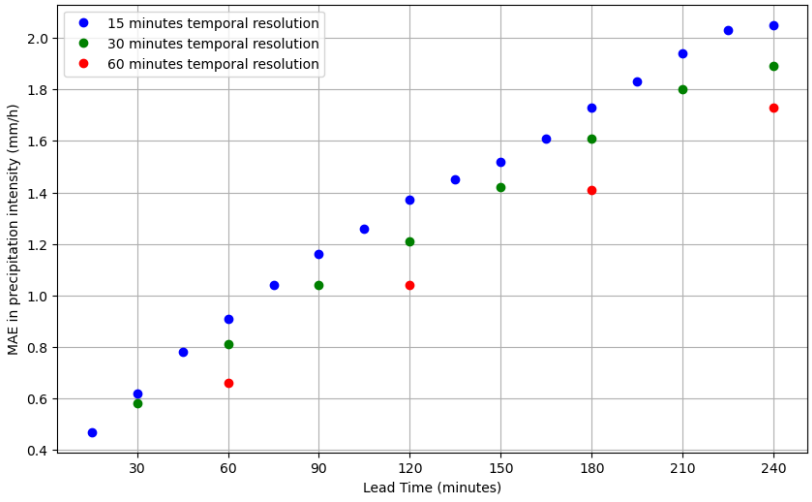


***Figure 18 Mean Absolute Error of 116 precipitation events > 5.0 mm/h in Odaw basin for various temporal resolutions in input data***

***Table 8 Maximum skillful lead time of S-PROG nowcast in Ghana for various spatial scale levels and temporal resolutions of the MSG-CPP IR input data***

| **Spatial scale level FSS** | **Maximum skillful lead time** | | | | | |
|---|---|---|---|---|---|---|
| | **Median** | **75% percentile** | **Median** | **75% percentile** | **Median** | **75% percentile** |
| | *15 min temporal resolution* | | *30 min temporal resolution* | | *60 min temporal resolution* | |
| **3 km** | 30 min | 0 min | 30 min | 0 min | 0 min | 0 min |
| **9 km** | 45 min | 15 min | 30 min | 0 min | 0 min | 0 min |
| **60 km** | 90 min | 45 min | 90 min | 30 min | 60 min | 0 min |
| **180 km** | 120 min | 60 min | 120 min | 30 min | 60 min | 0 min |
| **300 km** | 135 min | 60 min | 120 min | 30 min | 60 min | 0 min |

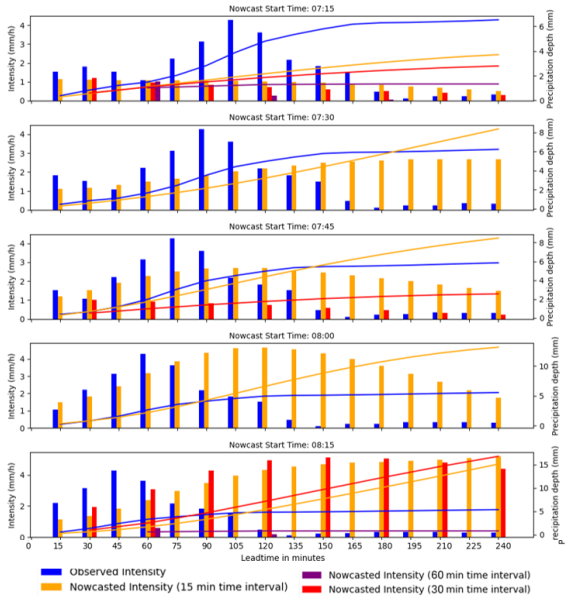


*Figure 19 Observed and nowcasted precipitation for a 15- 30- and 60-minute temporal resolution of input data 10/05/2020, the lines represent cumulative rainfall depth*

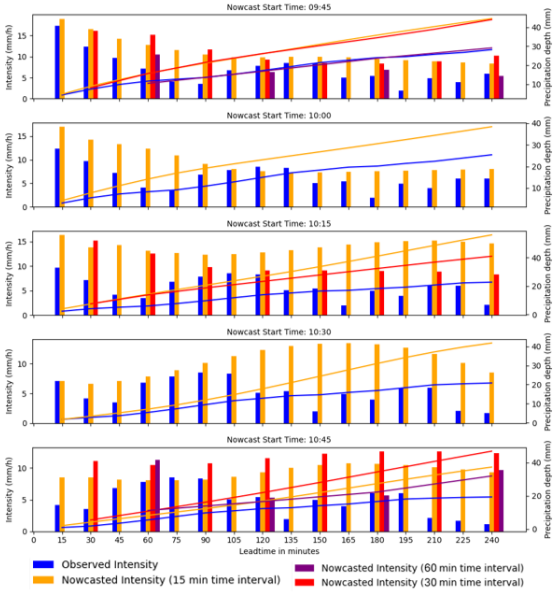


*Figure 20 Observed and nowcasted precipitation for a 15- 30- and 60-minute temporal resolution of input data 26/05/2020 the lines represent cumulative rainfall depth*

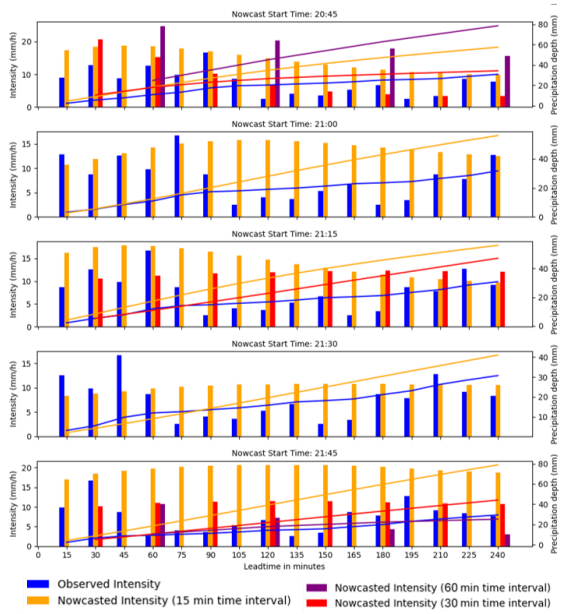


*Figure 21 Observed and nowcasted precipitation for a 15- 30- and 60-minute temporal resolution of input data 21/05/2022 the lines represent cumulative rainfall depth*

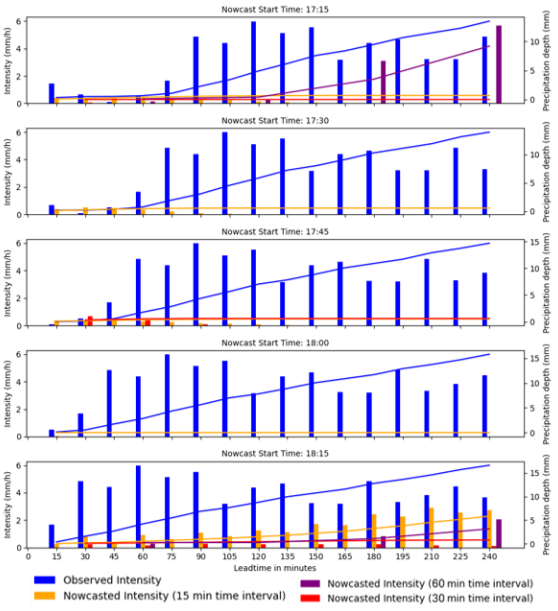


*Figure 22 Observed and nowcasted precipitation for a 15- 30- and 60-minute temporal resolution of input data 27/04/2023 the lines represent cumulative rainfall depth*

the precipitation peak while the 15- and 30-minute nowcast completely miss it, see figure 22.

# 4. Discussion and recommendations

The research presented in this MSc thesis aimed to assess the accuracy and suitability of satellite-based precipitation products for nowcasting in the Republic of Ghana. In this section, the limitations of the used research set-up are discussed and the results are compared with available literature. Moreover, the practical implications of the results for operational early warning purposes are described. Finally, recommendations are given for future research, where a differentiation has been made in short-term and relatively easy applicable research steps and a long-term research vision to strive towards reliable nowcasting using satellite-based data sources.

***Limitations of research set-up***

The research method comes with several limitations. Firstly, to analyze the detection capabilities of the MSG-CPP retrieval products, a comparison is made between point measurement data and pixel values that represent mean precipitation estimates over a pixel domain. In this study, the detection of precipitation (> 0.1 mm/h) and the detection of peak precipitation intensities is evaluated. This 0.1 mm/h threshold is selected based on the stated accuracy level of the TAHMO stations. Nevertheless, questions can be raised concerning the accuracy level for such small precipitation intensities, especially in regions with high evapotranspiration rates. Furthermore, the peak intensity threshold was set at the 95% percentile of the measured TAHMO precipitation data over the 19 stations in Ghana. For the MSG-CPP products, a threshold percentile of 90% was utilized. In these peak threshold definitions, no differentiation is made addressing seasonality or local climate variations. Additionally, no research is performed to indicate which precipitation intensities could cause flash floods in the study area. The TAHMO dataset is used as the only data source of in situ data in the region. In the comparative analysis of the different retrieval products, it was visible that TAHMO consistently shows much lower rainfall intensities than the different retrieval products. This raises questions about the accuracy of the TAHMO measurements. In the scope of this study, the TAHMO data is not validated in relation to other ground measurements.

Moreover, the MSG-CPP data is the only included retrieval product which is based on the geostationary Meteosat data. The other considered retrieval products are derived from data of orbiting satellites. The results of this study show a limited ability of the MSG-CPP retrieval product to represent TAHMO precipitation measurements in Ghana. To assess the potential of precipitation representation using Meteosat data, it would be a valuable addition to add another retrieval product that uses Meteosat data as a basis for rainfall retrieval, for example, the EUMESAT H60B data. This retrieval product also uses Meteosat data as the main data source, however precipitation intensities are calibrated using microwave data of orbiting satellites (EUMETSAT HSAF, 2019).

Additionally, the comparison of precipitation peak data for the Odaw catchment comes with some remarks. Firstly, not the exact basin boundaries, but a square boundary around the catchment was used. Moreover, the measured TAHMO intensity data of the Odaw catchment is derived using only three measurement points and the usage of Thiessen polygons. The usage of Thiessen polygons is a simplified view of reality. The results are highly sensitive to the accuracy of the three measurement stations. Preferably, a higher density of measurement stations and ground-radar equipment would be used to measure and compare precipitation intensities.

In the nowcast analyses emphasis is given on precipitation events with a precipitation intensity > 5.0 mm/h. This focus hinders the generalization of the conclusion for precipitation events with lower intensities. Additionally, the study set-up utilized the deterministic S-PROG nowcasting method. Using a deterministic approach limits the understanding of uncertainties related to the nowcasting results. For future research, it would be interesting to analyze the difference in nowcasting skill between the deterministic S-PROG and stochastic STEPS method using satellite-based retrieval products. Moreover, it would be valuable to analyze the propagation of uncertainties originating from the retrieval algorithm and assess which effect they have on the reliability of the nowcasting results.

***Research results in a literature perspective***

Roebeling & Holleman, (2009), who developed the MSG-CPP visual algorithm, used Dutch radar data from May and June 2007 to validate their product. For a selection of events, they observed a precipitation POD between 32% and 67%. In the presented research results for Ghana the POD for precipitation (> 0.1 mm) is 81% using MSG-CPP visual. For the detection of peak intensities, this POD is reduced to 39%. Due to the limited period over which Roebeling & Holleman (2009) validated their algorithm, their calibration had likely limited focus on peak precipitation. This can explain the difference in POD for the overall and peak precipitation. The master thesis of Brasjen (2014) describes the development of the Nighttime Infrared Precipitation Estimation (NIPE) algorithm, which produces the MSG-CPP IR data. The thesis presented a 24% accuracy in classifying a satellite pixel as precipitating or non-precipitation for the Dutch weather. Moreover, the precipitation estimates deviated on average by a factor of 3.3 from radar observations. For Ghana, the 95% percentile precipitation intensity of THAMO and MSG-CPP IR deviated by a factor of 2.1. Moreover, Brasjen (2014) describes that the number of

precipitation events in the NIPE algorithm is slightly overestimated. This overestimation could explain the high number of false alarms that were detected in the peak analyses. Nevertheless, this study found a FAR of 0.75, this can be interpreted as more than just a "slight" overestimation in rainfall events. In 2017, Meiring & Brasjen aimed to improve the MSG-CPP IR algorithm using GPM radar data. For detecting precipitation, a CSI of 22% was derived. This study derived a CSI of 20% for detecting precipitation with the MSG-CPP IR retrieval data. For the detection of peak intensities, this CSI reduced to 4%. Meiring & Brasjen (2017) state that their precipitation rate estimates deviated on average by a factor of 3.5 from the GPM observations and are unbiased.

Bogerd et al., (2024) presented the first paper in which the MSG-CPP visual and IR retrieval products are compared with ground measurements in Ghana. The study concludes an extreme overestimation of precipitation intensities in the MSG-CPP visual algorithm. The MSG-CPP IR data show a precipitation intensity with a factor of 1.5 higher in the wet season compared to TAHMO. This is in line with the observations of this study. Interesting is that, despite the extreme overestimations in rainfall intensity, Bogerd et al., (2024) detect a higher correlation between the TAHMO and MSG-CPP visual data compared to the correlation with MSG-CPP IR data. Also, in the results of this research, the POD for the visual retrieval product is higher than for the IR product.

According to Bogerd et al., (2024), the IMERG late retrieval data agrees in annual sums, and on basin scale for seasonal and daily resolutions with TAHMO observations. Nevertheless, capturing the strong spatial variability of rainfall and detecting high-intensity events is challenging. Dezfuli et al., (2017) analyzed the IMERG performances over the complete African continent with the usage of TAHMO stations. A main conclusion was that the IMERG performance highly varies per season and region. This conclusion underlines the need for local calibration of satellite-based rainfall retrieval products. Atiah et al., (2020) and Owusu et al., (2019) researched the accuracy of the CMORPH retrieval product for Ghana. Both studies indicate an overestimation of precipitation intensity. This is in line with the findings of this research. Nevertheless, Atiah et al., (2020) described an underestimation of the most extreme events. This is something that was not observed for the eight selected peak events in this study.

Burton et al., (2022) applied the S-PROG method with Meteosat data to generate satellite-derived convective rain rates for West Africa. On a 10-km resolution, skillful performances up to 2 hours lead times were detected. For a resolution of 200 km, the skillful lead times increase up to 4 hours. The research shows a large diurnal variation in nowcasting performances. Another paper that elaborates on the accuracy of satellite extrapolation nowcasting is presented by Hill et al., (2020). This research evaluated the convective rainfall rate (CRR) and rapidly developing thunderstorm convection warning (RDT-CW) for nowcasting in tropical Africa. Both methods show skillful lead times up to 90 minutes. Imhoff et al., (2020) applied four different nowcasting algorithms for 1533 precipitation events in the Netherlands. For the S-PROG method, a skillful lead time of 37 minutes was defined for a 10 km scale. The Ghana nowcast results in this research show a skillful lead time between 30 and 45 minutes on a scale of 9 km. This is in line with the findings of Imhoff et al., (2020), however, it is much shorter than the results of Burton et al., (2022) and Hill et al., (2020). The exact cause of this difference is uncertain.

***Practical implications of research results***

In the scope of this study, the validity of the TAHMO measurements is not evaluated. For the practical implications of the research results, the assumption is made that the TAHMO data correctly represents reality. Nevertheless, it is strongly recommended to test this assumption using more and other sources of in situ data. The detection analyses using TAHMO data showed that the current MSG-CPP IR and visual algorithm have a limited detection ratio and a high false alarm ratio. Moreover, they significantly overestimate precipitation intensities compared to ground-based observations. Bias-correcting the intensities is considered ineffective due to the low detectability of the peak precipitation events. Based on these results questions can be raised concerning the applicability of the current MSG-CPP products for operational nowcasting and early warning. Nevertheless, it is important to consider the reference situation in which there is currently no operational nowcast data available in Ghana. To weigh the potential advantages and disadvantages of applying the MSG-CPP retrieval products for early warning purposes the social-economic effects and action perspective need to be assessed by local experts and decision makers. Import to consider is that the uncertainties in the retrieval products

will further increase when they propagate through the nowcasting workflow.

When comparing the different precipitation retrieval products for the Odaw basin, it was visible that the MSG-CPP IR, IMERG Early, IMERG Final, and CMORPH data show similar performances in representing rainfall in relation to the TAHMO observations. This is remarkable especially because the IMERG final and CMORPH retrieval products make use of detailed microwave data and extensive postprocessing which is not performed for MSG-CPP IR and IMERG Early. This observation underlines the complexity of composing reliable precipitation estimates from satellite products. However, it also provides perspective on the usage of Meteosat-based retrieval products. Within the scope of this research, the MSG-CPP IR product showed comparable results to the advanced IMERG and CMORPH products, with the added benefit of operational applicability.

In this study, the MSG-CPP IR retrieval product is used for the nowcast evaluation. The practical usage of the MSG-CPP visual data is hindered due to its dependence on daylight. During the wet season, approximately 30% of the precipitation events occur at night and would consequently not be detected by the MSG-CPP visual retrieval product (Bogerd et al., 2024). Additionally, the IMERG Early product could be considered for operational nowcasting. However, its latency of 4 hours is expected to have a significant impact on the practical usage of derived nowcast results. The MSG-CPP IR S-PROG nowcasting results for Ghana show FSS indicators with large performance variability. Nevertheless, median skillful nowcast performances are observed for 45, 90, 120, and 135 minutes of lead times for the respective scale levels of 9-, 60-, 180-, and 300 km. The MSG-CPP data has a latency of just 45 minutes. This implies that operational applicability of the S-PROG nowcast using satellite data could be feasible. Additionally, it was observed that the nowcast results are sensitive to the temporal resolution of input data. The FSS performance indicator showed that the spatial patterns for precipitation are better represented using higher temporal resolutions in the input data. However, for the estimation of precipitation intensities, lower resolution input data led to better MAE evaluations. This is remarkable and potentially caused by the reduced extrapolation of precipitation patterns. From a practical perspective, it could be beneficial to compose a combination of nowcast results using various spatial resolutions to optimize the representation of the spatial patterns, as well as the precipitation intensity estimates.

***Recommended next research steps***

To better understand the detectability and accuracy of satellite-based retrieval products it is recommended to increase the number of ground measurement stations in the analyses. In this study, the TAHMO observations show much lower precipitation intensities than the retrieval products. Adding more ground measurements, for example from the Ghana Meteorological Agency (GMET), is useful to validate the accuracy of the TAHMO measurements. Additionally, it is suggested to perform the event precipitation analyses, as executed for the Odaw catchment, also for other basins in Ghana. This analysis would provide insight into whether the overestimation of precipitation intensities in the retrieval products is landscape or climate-zone-dependent. Furthermore, a sensitivity analysis based on seasonality would be an interesting addition. These results are of high value to research the transferability and generalizability of the research results. Moreover, in this study, a focus was given on retrieval products with a small temporal resolution (max 30 minutes). The S-PROG nowcasting results showed to be sensitive to the temporal resolution of the input data. However, skillful performances are observed for input data with temporal resolutions of 30 and 60 minutes. Based on this observation it could be of value to include additional retrieval products with a coarser temporal resolution (e.g. PERSIANN, GSMaP V5/6 & EUMESAT H60B) to the comparative analyses of retrieval products.

From an overarching perspective, this study aimed to contribute to operational and accessible early warning for extreme precipitation in areas with limited ground radar data. To strive towards this overarching goal, the following research steps are recommended. Firstly, the MSG-CPP algorithm shows high potential for nowcasting in the public domain as it has the shortest latency and highest temporal and spatial resolution. However, its correspondence with TAHMO measurements in Ghana is currently limited. Besides validating the accuracy of the TAHMO stations, a recommended next research step is to improve the MSG-CPP algorithm using a localized calibration approach and the usage of ground measurements. When the algorithm was developed in 2014, its calibration set-up was focused

on the Dutch climate. Later Brasjen & Meirink (2017) calibrated the IR-based algorithm using GPM radar data. In this calibration, no specific focus was given to the representation of variating climates. The NIPE algorithm first composes a cloud classification and subsequently derives a precipitation intensity based on this cloud class. Potentially, the classification of clouds and the associated precipitation statistics are different for various climates. To get a better understanding of the accuracy of the retrieval product based on the cloud types it is useful to have access to a historical time series of cloud classifications. When the uncertainty of precipitation retrieval can be linked to specific cloud classes, it could be possible that the MSG-CPP algorithm does not only provide rainfall maps but also corresponding uncertainty indicators. These uncertainty indicators can be used in the nowcasting set-up and the decision making process concerning early warning communication. Another point of attention in the calibration of the NIPE algorithm is that Brasjen & Meirink (2017) used a data archive of only one year. This data was subsequently also split into a calibration and validation dataset. This implies that the number of high-intensity precipitation events included in current algorithm calibration is likely limited.

Additionally, Bogerd et al., (2024) address two potential causes for deviations between the MSG-CPP retrieval products and ground measurements. Firstly, evaporation of precipitation before the ground is reached. In warm tropical climates evaporation can be significant. Precipitation which evaporates before it reaches the ground is not detected by the TAHMO stations and this can therefore be the cause of inconsistencies between the rainfall retrieval products and the ground measurements. In future research, the effect of evaporation can be analyzed by including temperature or humidity data and correlating this to the variations between the retrieval products and ground measurements. A potential next uncertainty source is the presence of “Harmattan Dust” in Ghana. This is a very dry and dust-laden wind that blows at a height of 3 km (Breuning-Madsen & Awadzi, 2005). Harmattan dust could cause increased evaporation rates during the dry season and could also be incorrectly classified as clouds (Bogerd et al., 2024).

The current MSG-CPP visual algorithm has a higher detectability of peak precipitation intensity than the IR product. However, the IR product shows a larger correspondence in precipitation estimates. Potentially these observations can be used as a starting point to increase the quality of the algorithm. It is advised to dominantly focus on an algorithm structure that enables continuous precipitation retrieval. For nowcasting and early warning purposes, daylight dependence is impractical.

Besides improving the retrieval product, it is recommended to do more in-depth research concerning the exact nowcasting method which is applicable for satellite-based rainfall data. In this study the basic set-up of the deterministic S-PROG method as developed by Seed, (2003) is used. A study by Imhoff et al., (2020) shows high nowcasting skills for the stochastic STEPS method. It would be interesting to analyze the nowcasting skill of the STEPS method using satellite-based retrieval products as input. Besides, it is advised to analyze the nowcast sensitivity on various settings of the S-PROG algorithm. For example, various optical flow methods, different quantities of spatial cascades, and varying numbers of timesteps to derive the nowcasting motion field. Especially this last variable is of interest because the sensitivity analyses of the temporal resolution showed indications that the inclusion of a larger timeframe as input data could lead to less extreme extrapolations of precipitation intensities.

Finally, to facilitate operational early warning, seamless precipitation prediction is of high value. Seamless predictions of precipitation go beyond the six hours of lead time which fall under the nowcasting definition. Studies by Imhoff et al., (2023), Nerini et al., (2019) and Radhakrishnan & Chandrasekar, (2020) show promising developments in the field of blended weather predictions in which (radar-based) nowcasts and NWP models are combined to create a seamless weather model. It would be interesting to apply these blending algorithms using satellite-based nowcasting data and an NWP model.

# 5. Conclusion

Reliable precipitation nowcasting data is of high value for early warning purposes. Availability of such data is for many regions on the African continent hindered due to the lack of ground-radar data. Satellite-based precipitation products offer potential to be used for nowcasting purposes in areas with scarce radar coverage. This study assessed the accuracy and suitability of satellite-based

precipitation products for nowcasting purposes in the Republic of Ghana. In this research, a focus is given to the MSG-CPP infrared (IR) and visual retrieval products. These products show high potential for operational nowcasting purposes due to their relatively short latency (45 min) and high temporal (15 min) and spatial resolution (3 km). Additionally, CMORPH, IMERG Early, and Final are included as reference satellite-based products. Furthermore, data from 19 TAHMO ground measurement stations are used as in situ data.

***Accuracy of the MSG-CPP rainfall retrieval products in Ghana***

The accuracy of the MSG-CPP products is analyzed on a 15-minute temporal resolution over a timeseries of 35 months while using the TAHMO measurements as a reference. This resulted in a Probability Of Detecting (POD) for precipitation of 49% for the IR and 81% for the visual retrieval product. Additionally, the detection capabilities for peak precipitation are examined. In the scope of this research, the 95% percentile precipitation intensity of TAHMO observations is used as peak intensity threshold. This resulted in a POD of 19% for the IR and 39% for the visual product. Additionally, both retrieval products are subject to high false alarm ratios (FAR). The MSG-CPP algorithm has a FAR of 75% for precipitation detection and for 95% for peak precipitation. For the MSG-CPP visual these FAR performance indicators are respectively 80% and 93%. When comparing the 95% percentile intensities of MSG-CPP products with TAHMO observations, the MSG-CPP IR product shows an average overestimation with a factor of 1.7 and the visual product with a factor of 4.6.

***Comparative analyses of satellite-based retrieval products and TAHMO measurements for the Odaw basin, Ghana***

For eight heavy precipitation events in the Odaw basin in Ghana, the precipitation correspondence of the various retrieval products was compared with TAHMO ground measurements. This analysis showed that specifically the MSG-CPP visual product extremely overestimates the observed rainfall depths. The other retrieval products all show cumulative overestimations up to 500% in 24 hours. The precipitation start, end, and peak time varies up to 1.5 hours between the retrieval products. Moreover, the analyses showed that the retrieval products with short latencies (IMERG Early and MSG-CPP IR) show equal abilities in representing TAHMO observations compared to products with longer latencies (IMERG Final and CMORPH). This raises questions concerning the accuracy of the TAHMO stations, which was not verified within this study.

***S-PROG Nowcast results based on MSG-CPP IR input data***

The deterministic S-PROG nowcasting method is applied using the MSG-CPP IR data as input. The nowcasting results for precipitation events >5 mm/h show a large variance in nowcasting skill over the various events. Median skillful nowcast performances are observed for 45-, 90-, 120- and 135 minutes of lead times for the respective spatial scale levels of 9-, 60-, 180-, and 300 km. The MSG-CPP data has a latency of just 45 minutes. This implies that the operational applicability of the S-PROG nowcast using MSG-CPP satellite data could be feasible. Moreover, a sensitivity to the temporal resolution of the input data is detected. For operational applicability, it is important to perform additional research concerning the propagation of uncertainties originating from the retrieval product into the nowcast.

***Implications of research results***

The results of this study provide insights concerning the potential that satellite-based precipitation nowcasting has to offer. Critical evaluation of the TAHMO station accuracy and the MSG-CPP retrieval algorithm is recommended. It is expected that local calibration efforts using in situ data and a calibration focus on high precipitation intensities will increase the accuracy of the MSG-CPP products. Additionally, the S-PROG nowcasting results show promising results with skillful lead times which exceed the latency of the MSG-CPP data. Furthermore, the set-up of the nowcast model offers the potential for additional optimization of the modeling parameters.

Satellite-based operational precipitation nowcasting is of high value for disaster risk mitigation efforts in regions without ground-radar data. This study aims to underline the large potential of satellite-based precipitation nowcasting while being transparent concerning the remaining uncertainties. Within this novel research field, it is expected that additional research efforts can significantly contribute to the increased accessibility and reliability of operational precipitation nowcasting data.

## Acknowledgements

I would like to thank all people at HKV for introducing me into your team and providing me with support during this research. Specifically, I wish to express my appreciation to Dorien Lugt, Ruud Hurkmans and Jerom Aerts for your

kind and enthusiastic support as well as valuable insights. Additionally, I want to sincerely thank Martijn Booij and Tom Rientjes for their guidance and feedback during the research process. A special acknowledgement goes to Ruben Imhoff of Deltares whose nowcasting expertise was of great value to introduce me into this novel research field. Finally, I want express my gratitude to the TAHMO organization for granting access to their in-situ rainfall data. Without their contribution, this research would not have been possible.

# References


Aryee, J. N. A., Ahiataku, M. A., Quagraine, K. T., Davies, P., Agbenor-Efunam, N., Agyapong, G., Agyekum, J., Donkor, M. K. E., Osei, M. A., Poku, L. P., Amekudzi, L. K., Danuor, S. K., Ahiataku, M. A., Gloria, A., Poku, L. P., Aryee, J. N. A., Quagraine, K. T., Davies, P., Agbenor-Efunam, N., Danuor, S. K. (2022). High-impact weather (hiw) forecasting in Ghana: challenges and prospects of the nowcasting satellite facility (nwcsaf) for improved early warning and decision-making.https://doi.org/10.22541/au.165712587.76658353/v1

Atiah, W. A., Tsidu, G. M., & Amekudzi, L. K. (2020). Investigating the merits of gauge and satellite rainfall data at local scales in Ghana, West Africa. *Weather and Climate Extremes*, *30*, 100292. https://doi.org/10.1016/j.wace.2020.100292

Ayzel, G., Heistermann, M., & Winterrath, T. (2019). Optical flow models as an open benchmark for radar-based precipitation nowcasting (rainymotion v0.1). *Geoscientific Model Development*, *12*(4). https://doi.org/10.5194/gmd-12-1387-2019

Benas, N., Finkensieper, S., Stengel, M., Van Zadelhoff, G. J., Hanschmann, T., Hollmann, R., & Meirink, J. F. (2017). The MSG-SEVIRI-based cloud property data record CLAAS-2. *Earth System Science Data*, *9*(2). https://doi.org/10.5194/essd-9-415-2017

Beusch, L., Foresti, L., Gabella, M., & Hamann, U. (2018). Satellite-based rainfall retrieval: From generalized linear models to artificial neural networks. *Remote Sensing*, *10*(6). https://doi.org/10.3390/rs10060939

Bogerd, L., Pinto, R. B., Leijnse, H., Meirink, J. F., van Emmerik, T. H. M., & Uijlenhoet, R. (2024). Gauging the ungauged: estimating rainfall in a West African urbanized river basin using ground-based and spaceborne sensors. *Hydrological Sciences Journal*, *69*(2), 259–273. https://doi.org/10.1080/02626667.2023.2284871

Bowler, N. E., Pierce, C. E., & Seed, A. W. (2006). STEPS: A probabilistic precipitation forecasting scheme which merges an extrapolation nowcast with downscaled NWP. *Quarterly Journal of the Royal Meteorological Society*, *132*(620). https://doi.org/10.1256/qj.04.100

Brasjen, A. M. (2014). Precipitation estimation from infrared satellite imagery*, TU Delft MSc thesis*.

Brasjen, N. 'Meirink, J. F. (2017). *Feasibility of cloud microphysics based precipitation retrievals for nowcasting, CDOP2 WP22600 End Report*.

Breuning-Madsen, H., & Awadzi, T. W. (2005). Harmattan dust deposition and particle size in Ghana. *CATENA*, *63*(1), 23–38. https://doi.org/10.1016/j.catena.2005.04.001

Bruce, L. and T. K. (1981). An Iterative Image Registration Technique with an Application to Stereo Vision. *7th International Joint Conference on Artificial Intelligence,* 674–679.

Burton, R., Blyth, A. M., Cui, Z., Groves, J., Lamptey, B. L., Fletcher, J. K., Marsham, J. H., Parker, D. J., & Roberts, A. (2022). Satellite-Based Nowcasting of West African Mesoscale Storms Has Skill at up to 4-h Lead Time. *Weather and Forecasting*, *37*(4). https://doi.org/10.1175/WAF-D-21-0051.1

Clark, A. J., Gallus, W. A., Xue, M., & Kong, F. (2009). A comparison of precipitation forecast skill between small convection-allowing and large convection-parameterizing ensembles. *Weather and Forecasting*, *24*(4). https://doi.org/10.1175/2009WAF2222222.1

Codjoe, S. N. A., & Atiglo, D. Y. (2020). The Implications of Extreme Weather Events for Attaining the Sustainable Development Goals in Sub-Saharan Africa. In *Frontiers in Climate* (Vol. 2). https://doi.org/10.3389/fclim.2020.592658

Dezfuli, A. K., Ichoku, C. M., Huffman, G. J., Mohr, K. I., Selker, J. S., van de Giesen, N., Hochreutener, R., & Annor, F. O. (2017). Validation of IMERG precipitation in Africa. *Journal of Hydrometeorology*, *18*(10). https://doi.org/10.1175/JHM-D-17-0139.1

Dinku, T., Connor, S. J., & Ceccato, P. (2010). Comparison of CMORPH and TRMM-3B42 over mountainous regions of Africa and South America. In *Satellite Rainfall Applications for Surface Hydrology*. https://doi.org/10.1007/978-90-481-2915-7_11

*ECMWF*. (2023). Https://Www.Ecmwf.Int/.

EUMETSAT H SAF. (2019). *Algorithm Theoretical Baseline Document (ATBD) for product H60 P-IN-SEVIRI-PMW, H63 P-IN_SEVIRI_PMW_E*.

Foresti, L., Sideris, I. V., Nerini, D., Beusch, L. E. A., & Germann, U. R. S. (2019). Using a 10-year radar archive for nowcasting precipitation growth and decay: A probabilistic machine learning approach. *Weather and Forecasting*, *34*(5). https://doi.org/10.1175/WAF-D-18-0206.1

Germann, U., & Zawadzki, I. (2002). Scale-Dependence of the Predictability of Precipitation from Continental Radar Images. Part I: Description of the Methodology. *Monthly Weather Review*, *130*(12), 2859–2873. https://doi.org/10.1175/1520-0493(2002)130<2859:SDOTPO>2.0.CO;2

Greuell, W., Meirink, J. F., & Wang, P. (2013). Retrieval and validation of global, direct, and diffuse irradiance derived from SEVIRI satellite observations. *Journal of Geophysical Research Atmospheres*, *118*(5). https://doi.org/10.1002/jgrd.50194

Hamill, T. M., Hagedorn, R., & Whitaker, J. S. (2008). Probabilistic forecast calibration using ECMWF and GFS ensemble reforecasts. Part II: Precipitation. *Monthly Weather Review*, *136*(7). https://doi.org/10.1175/2007MWR2411.1

Hill, P. G., Stein, T. H. M., Roberts, A. J., Fletcher, J. K., Marsham, J. H., & Groves, J. (2020). How skilful are Nowcasting Satellite Applications Facility products for tropical Africa? *Meteorological Applications*, *27*(6). https://doi.org/10.1002/met.1966

Honda, T., Amemiya, A., Otsuka, S., Taylor, J., Maejima, Y., Nishizawa, S., Yamaura, T., Sueki, K., Tomita, H., & Miyoshi, T. (2022). Advantage of 30-s-Updating Numerical Weather Prediction With a Phased-Array Weather Radar Over Operational Nowcast for a Convective Precipitation System. *Geophysical Research Letters*, *49*(11). https://doi.org/10.1029/2021GL096927

Hou, A. Y., Kakar, R. K., Neeck, S., Azarbarzin, A. A., Kummerow, C. D., Kojima, M., Oki, R., Nakamura, K., & Iguchi, T. (2014). The global precipitation measurement mission. *Bulletin of the American Meteorological Society*, *95*(5). https://doi.org/10.1175/BAMS-D-13-00164.1

Huffman, G. J. , et al. (2020). *NASA Global precipitation measurement (GPM) integrated multi-satellitE retrievals for GPM (IMERG). Algorithm Theoretical Basis Doc.*

Imhoff, R. O., Brauer, C. C., Overeem, A., Weerts, A. H., & Uijlenhoet, R. (2020). Spatial and Temporal Evaluation of Radar Rainfall Nowcasting Techniques on 1,533 Events. *Water Resources Research*, *56*(8). https://doi.org/10.1029/2019WR026723

Imhoff, R. O., Brauer, C. C., van Heeringen, K. J., Uijlenhoet, R., & Weerts, A. H. (2022). Large-Sample Evaluation of Radar Rainfall Nowcasting for Flood Early Warning. *Water Resources Research*, *58*(3). https://doi.org/10.1029/2021WR031591

Imhoff, R. O., De Cruz, L., Dewettinck, W., Brauer, C. C., Uijlenhoet, R., van Heeringen, K. J., Velasco-Forero, C., Nerini, D., Van Ginderachter, M., & Weerts, A. H. (2023). Scale-dependent blending of ensemble rainfall nowcasts and numerical weather prediction in the open-source pysteps library. *Quarterly Journal of the Royal Meteorological Society*, *149*(753). https://doi.org/10.1002/qj.4461

Ivan Kuznetsov. (2023). *ECMWF vs GFS. What's the difference, and which weather model is more accurate*. Windy.App.

Joyce, R. J., Janowiak, J. E., Arkin, P. A., & Xie, P. (2004). CMORPH: A Method that Produces Global Precipitation Estimates from Passive Microwave and Infrared Data at High Spatial and Temporal Resolution. *Journal of Hydrometeorology*, *5*(3), 487–503. https://doi.org/10.1175/1525-7541(2004)005<0487:CAMTPG>2.0.CO;2

Kawo, N. S., Hordofa, A. T., & Karuppannan, S. (2021). Performance evaluation of GPM-IMERG early and late rainfall estimates over Lake Hawassa catchment, Rift Valley Basin, Ethiopia. *Arabian Journal of Geosciences*, *14*(4), 256. https://doi.org/10.1007/s12517-021-06599-1

Kikuchi, M., Braun, S. A., Suzuki, K., Liu, G., & Battaglia, A. (2022). Satellite Precipitation Measurements: What Have We Learnt About Cloud-Precipitation Processes From Space? *Cloud Physics and Dynamics: Showers and Shade from Earth's Atmosphere*.

Kobold, M., & Sušelj, K. (2005). Precipitation forecasts and their uncertainty as input into hydrological models. *Hydrology and Earth System Sciences*, *9*(4). https://doi.org/10.5194/hess-9-322-2005

Kummerow, C. D. (2020). Introduction to Passive Microwave Retrieval Methods. In *Advances in Global Change Research* (Vol. 67). https://doi.org/10.1007/978-3-030-24568-9_7

Larmie Seth. (2019). greater accra resilient and integrated development project. Worldbank.

Laura Wismans. (2023, August). Africaanse landen kunnen extreem weer vaak niet goed voorspellen. *NRC*.

Li, Z., Tang, G., Hong, Z., Chen, M., Gao, S., Kirstetter, P., Gourley, J. J., Wen, Y., Yami, T., Nabih, S., & Hong, Y. (2021). Two-decades of GPM IMERG early and final run products intercomparison: Similarity and difference in climatology, rates, and extremes. *Journal of Hydrology*, *594*, 125975. https://doi.org/10.1016/j.jhydrol.2021.125975

Logah, F. Y., Kankam-Yeboah, K., Ofori, D., & Gyau-Boakye, P. (2014). Flood pulse alterations of some river basins in Ghana.. In *Ghana J. Sci* (Vol. 54).

Maranan, M., Fink, A. H., Knippertz, P., Amekudzi, L. K., Atiah, W. A., & Stengel, M. (2020). A process-based validation of gpm imerg and its sources using a mesoscale rain gauge network in the west African forest zone. *Journal of Hydrometeorology*, *21*(4). https://doi.org/10.1175/JHM-D-19-0257.1

Medina, H., Tian, D., Marin, F. R., & Chirico, G. B. (2019). Comparing GEFS, ECMWF, and postprocessing methods for ensemble precipitation forecasts over Brazil. *Journal of Hydrometeorology*, *20*(4). https://doi.org/10.1175/JHM-D-18-0125.1

Mensah, H., & Ahadzie, D. K. (2020). Causes, impacts and coping strategies of floods in Ghana: a systematic review. In *SN Applied Sciences* (Vol. 2, Issue 5). https://doi.org/10.1007/s42452-020-2548-z

National Center for Environmental Information. (2023). *Global Forecast System (GFS)*. Https://Www.Ncei.Noaa.Gov/Products/Weather-Climate-Models/Global-Forecast.

Nerini, D., Foresti, L., Leuenberger, D., Robert, S., & Germann, U. (2019). A reduced-space ensemble kalman filter approach for flow-dependent integration of radar extrapolation nowcasts and NWP precipitation ensembles. *Monthly Weather Review*, *147*(3). https://doi.org/10.1175/MWR-D-18-0258.1

Ntajal, J., Höllermann, B., Falkenberg, T., Kistemann, T., & Evers, M. (2022). Water and Health Nexus—Land Use Dynamics, Flooding, and Water-Borne Diseases in the Odaw River Basin, Ghana. *Water*, *14*(3), 461. https://doi.org/10.3390/w14030461

Owusu, C., Adjei, K. A., & Odai, S. N. (2019). Evaluation of Satellite Rainfall Estimates in the Pra Basin of Ghana. *Environmental Processes*, *6*(1), 175–190. https://doi.org/10.1007/s40710-018-0344-1

Payne, T. J. (2017). Rapid update cycling with delayed observations. *Tellus, Series A: Dynamic Meteorology and Oceanography*, *69*(1). https://doi.org/10.1080/16000870.2017.1409061

Pierce, C., Seed, A., Ballard, S., Simonin, D., & Li, Z. (2012). Nowcasting. In J. Bech & J. L. Chau (Eds.), *Doppler Radar Observations*. IntechOpen. https://doi.org/10.5772/39054

Pradhan, R. K., Markonis, Y., Vargas Godoy, M. R., Villalba-Pradas, A., Andreadis, K. M., Nikolopoulos, E. I., Papalexiou, S. M., Rahim, A., Tapiador, F. J., & Hanel, M. (2022). Review of GPM IMERG performance: A global perspective. In *Remote Sensing of Environment* (Vol. 268). https://doi.org/10.1016/j.rse.2021.112754

Prigent, C. (2010). Precipitation retrieval from space: An overview. *Comptes Rendus - Geoscience*, *342*(4–5). https://doi.org/10.1016/j.crte.2010.01.004

Pulkkinen, S., Nerini, D., Pérez Hortal, A. A., Velasco-Forero, C., Seed, A., Germann, U., & Foresti, L. (2019). Pysteps: An open-source Python library for probabilistic precipitation nowcasting (v1.0). *Geoscientific Model Development*, *12*(10). https://doi.org/10.5194/gmd-12-4185-2019

Pysteps developers. (n.d.). *Cascade decomposition tutorial Pysteps*. Https://Pysteps.Readthedocs.Io/En/Latest/Auto_examples/Plot_cascade_decomposition.Html#sphx-Glr-Auto-Examples-Plot-Cascade-Decomposition-Py.

Radhakrishnan, C., & Chandrasekar, V. (2020). CASA prediction system over dallas–fort worth urban network: Blending of nowcasting and high-resolution numerical weather prediction model. *Journal of Atmospheric and Oceanic Technology*, *37*(2). https://doi.org/10.1175/JTECH-D-18-0192.1

Ravuri, S., Lenc, K., Willson, M., Kangin, D., Lam, R., Mirowski, P., Fitzsimons, M., Athanassiadou, M., Kashem, S., Madge, S., Prudden, R., Mandhane, A., Clark, A., Brock, A., Simonyan, K., Hadsell, R., Robinson, N., Clancy, E., Arribas, A., & Mohamed, S. (2021). Skilful precipitation nowcasting using deep generative models of radar. *Nature*, *597*(7878). https://doi.org/10.1038/s41586-021-03854-z

Roberts, N. M., & Lean, H. W. (2008). Scale-selective verification of rainfall accumulations from high-resolution forecasts of convective events. *Monthly Weather Review*, *136*(1). https://doi.org/10.1175/2007MWR2123.1

Roebeling, R. A., Feijt, A. J., & Stammes, P. (2006). Cloud property retrievals for climate monitoring: Implications of differences between Spinning Enhanced Visible and Infrared Imager (SEVIRI) on METEOSAT-8 and Advanced Very High Resolution Radiometer (AVHRR) on NOAA-17. *Journal of Geophysical Research Atmospheres*, *111*(20). https://doi.org/10.1029/2005JD006990

Roebeling, R. A., & Holleman, I. (2009). SEVIRI rainfall retrieval and validation using weather radar observations. *Journal of Geophysical Research Atmospheres*, *114*(21). https://doi.org/10.1029/2009JD012102

Seed, A. W. (2003). A dynamic and spatial scaling approach to advection forecasting. *Journal of Applied Meteorology*, *42*(3). https://doi.org/10.1175/1520-0450(2003)042<0381:ADASSA>2.0.CO;2

Shi, X., Chen, Z., Wang, H., Yeung, D. Y., Wong, W. K., & Woo, W. C. (2015). Convolutional LSTM network: A machine learning approach for precipitation nowcasting. *Advances in Neural Information Processing Systems*, *2015-January*.

Shi, X., Gao, Z., Lausen, L., Wang, H., Yeung, D. Y., Wong, W. K., & Woo, W. C. (2017). Deep learning for precipitation nowcasting: A benchmark and a new model. *Advances in Neural Information Processing Systems*, *2017-December*.

Smith, K. T., & Austin, G. L. (2000). Nowcasting precipitation - A proposal for a way forward. *Journal of Hydrology*, *239*(1–4). https://doi.org/10.1016/S0022-1694(00)00359-0

Sun, J., Xue, M., Wilson, J. W., Zawadzki, I., Ballard, S. P., Onvlee-Hooimeyer, J., Joe, P., Barker, D. M., Li, P. W., Golding, B., Xu, M., & Pinto, J. (2014). Use of nwp for nowcasting convective precipitation: Recent progress and challenges. *Bulletin of the American Meteorological Society*, *95*(3), 409–426. https://doi.org/10.1175/BAMS-D-11-00263.1

TAHMO. (2023). *TAHMO station manual 2023*. Https://Tahmo.Org/Wp-Content/Uploads/2023/06/TAHMOSTATIONmanual2023.Pdf.

Tan, J., Huffman, G. J., Bolvin, D. T., & Nelkin, E. J. (2019). IMERG V06: Changes to the Morphing Algorithm. *Journal of Atmospheric and Oceanic Technology*, *36*(12), 2471–2482. https://doi.org/10.1175/JTECH-D-19-0114.1

Tapiador, F. J., Navarro, A., García-Ortega, E., Merino, A., Sánchez, J. L., Marcos, C., & Kummerow, C. (2020). The Contribution of Rain Gauges in the Calibration of the IMERG Product: Results from the First Validation over Spain. *Journal of Hydrometeorology*, *21*(2), 161–182. https://doi.org/10.1175/JHM-D-19-0116.1

United Nations. (2023). *Early Warnings for All*. Https://Www.Un.Org/En/Climatechange/Early-Warnings-for-All#:~:Text=Early%20Warnings%20for%20All%20is,By%20the%20end%20of%202027.

van de Giesen, N., Hut, R., & Selker, J. (2014). The Trans-African Hydro-Meteorological Observatory, *WIREs Water*, *1*(4), 341–348. https://doi.org/10.1002/wat2.1034

van der Kooij, E. (2021). *Nowcasting Heavy Precipitation in the Netherlands: a Deep Learning Approach*. Msc thesis TU Delft.

Vannitsem, S., Bremnes, J. B., Demaeyer, J., Evans, G. R., Flowerdew, J., Hemri, S., Lerch, S., Roberts, N., Theis, S., Atencia, A., Bouallègue, Z. Ben, Bhend, J., Dabernig, M., de Cruz, L., Hieta, L., Mestre, O., Moret, L., Plenković, I. O., Schmeits, M., … Ylhaisi, J. (2021). Statistical postprocessing for weather forecasts review, challenges, and avenues in a big data world. In *Bulletin of the American Meteorological Society* (Vol. 102, Issue 3). https://doi.org/10.1175/BAMS-D-19-0308.1

Varma, A. K. (2018). Measurement of Precipitation from Satellite Radiometers (Visible, Infrared, and Microwave): Physical Basis, Methods, and Limitations. In *Remote Sensing of Aerosols, Clouds, and Precipitation*. https://doi.org/10.1016/B978-0-12-810437-8.00011-6

Weisman, M. L., Davis, C., Wang, W., Manning, K. W., & Klemp, J. B. (2008). Experiences with 0-36-h explicit convective forecasts with the WRF-ARW model. *Weather and Forecasting*, *23*(3). https://doi.org/10.1175/2007WAF2007005.1

World Bank Group. (2023). *Climate Change Knowledge Portal*.

# Appendix A: Precipitation retrieval products and TAHMO measurements for eight heavy rainfall events in Ghana

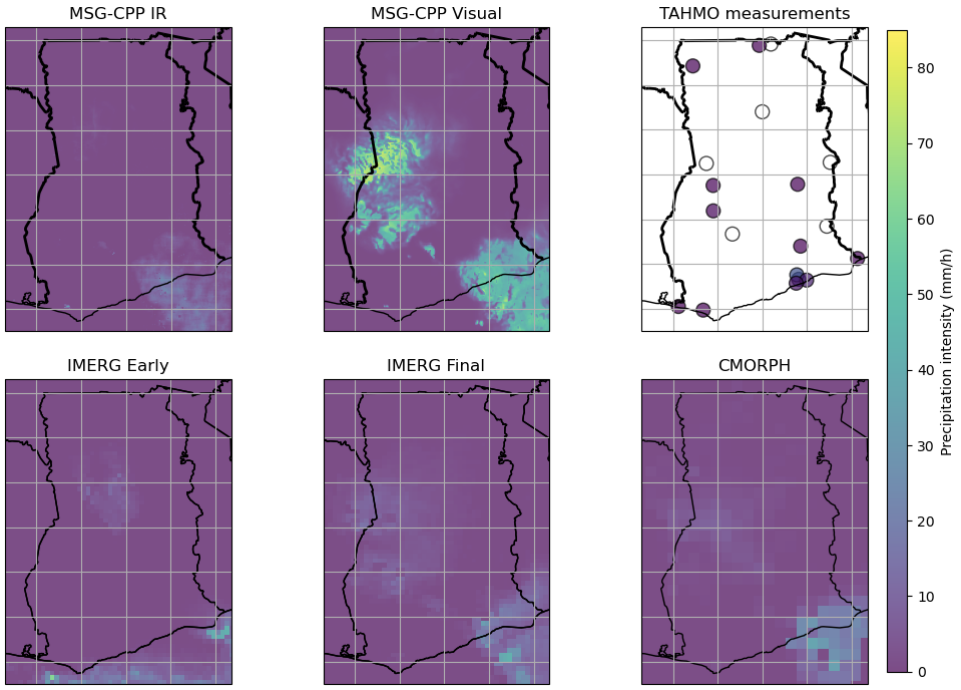


*(a) 26/04/2020 9:30*

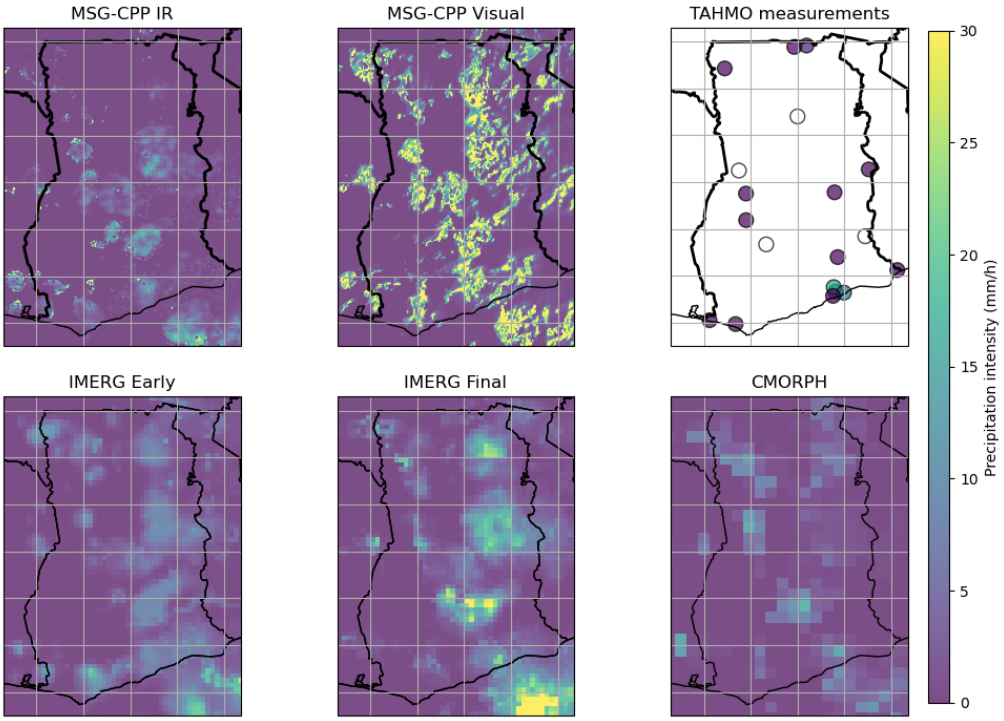


*(b) 10/05/2020 17:00*

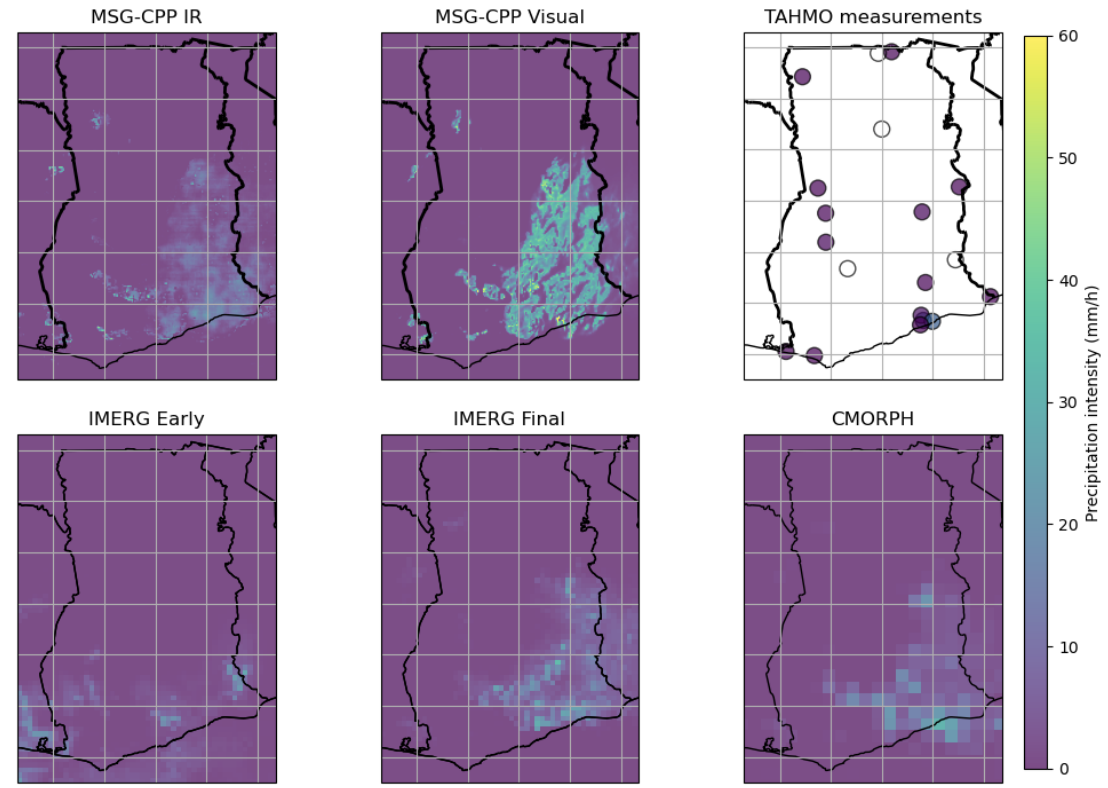


*(c) 28/05/2020 16:30*

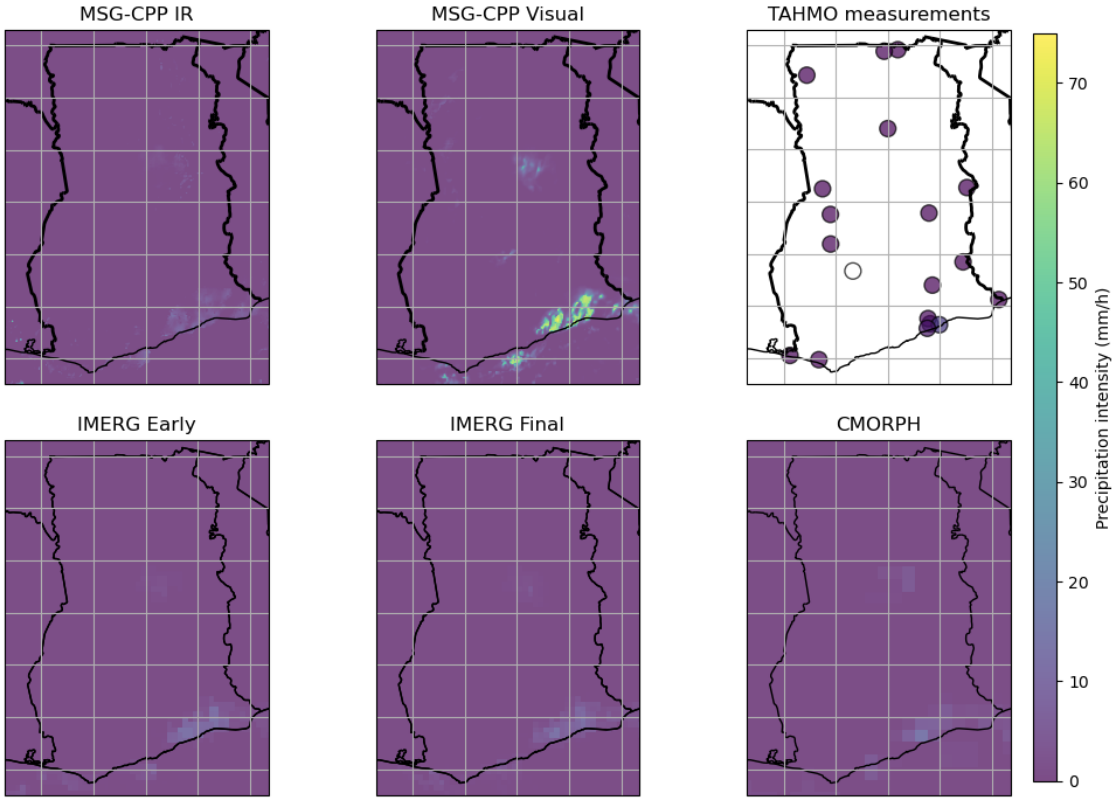


*(d) 10/10/2020 9:00*

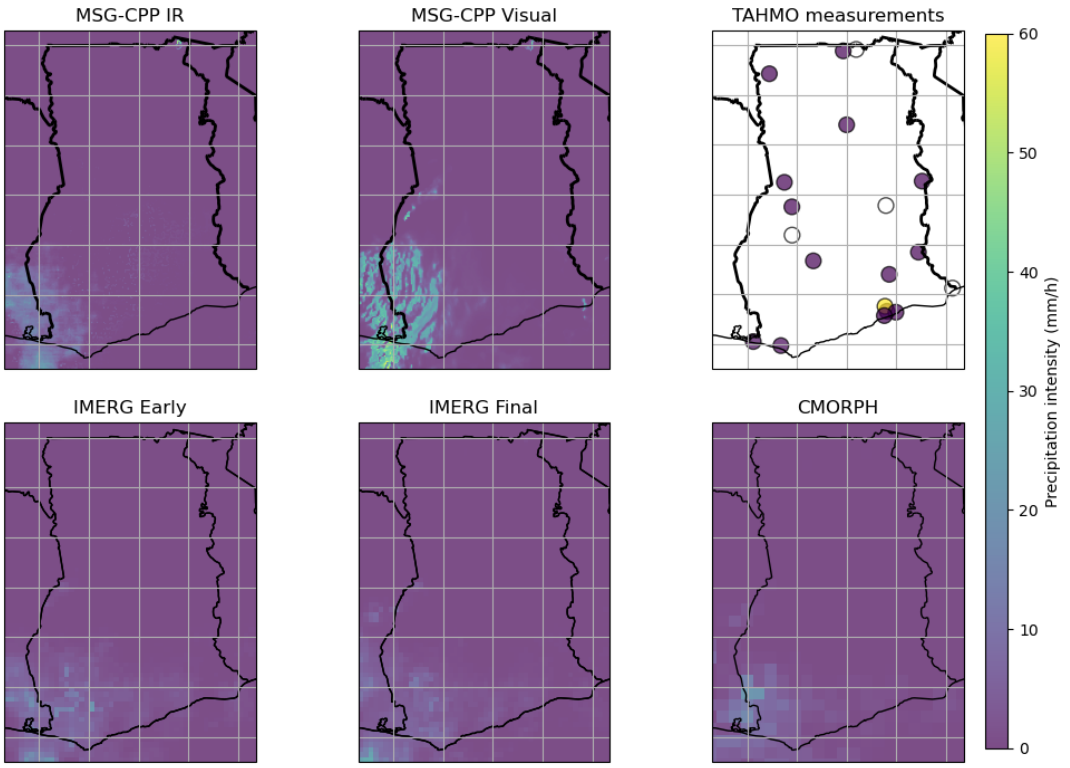


*(e) 06/05/2022 16:30*

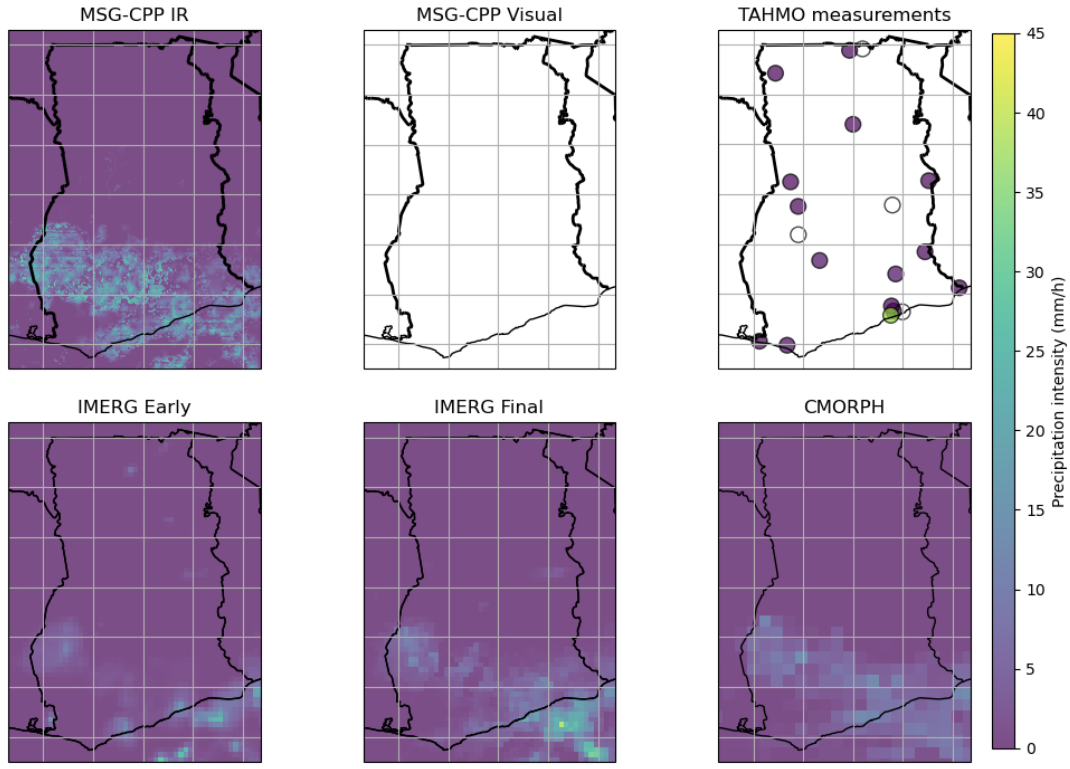


*(f ) 21/05/2021 20:30*

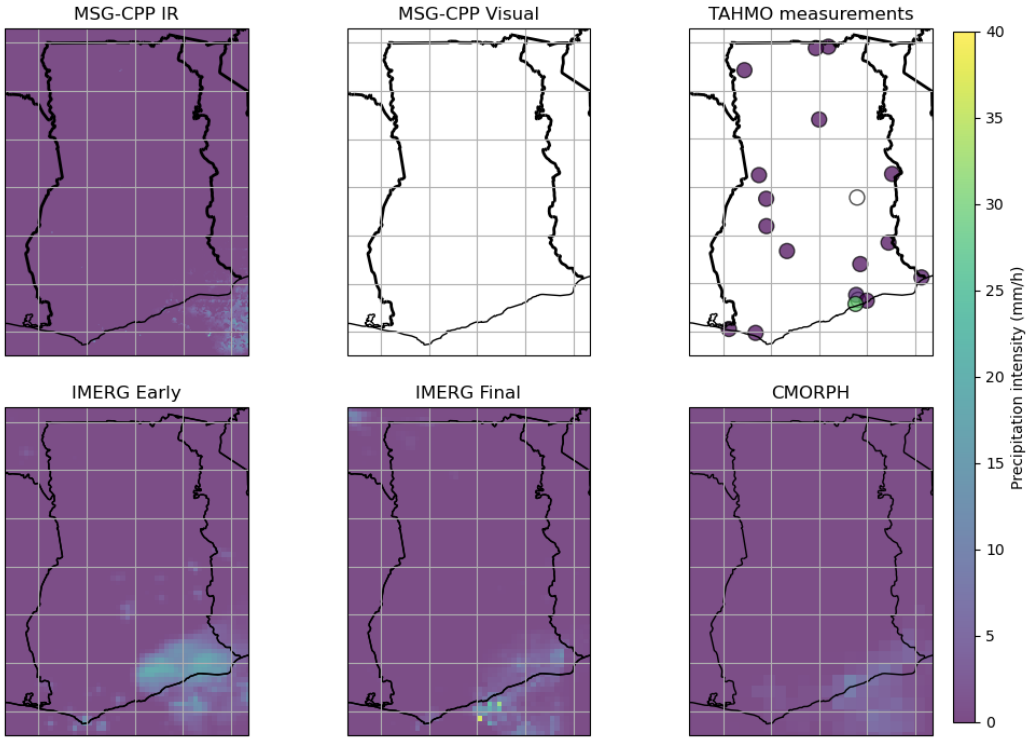


*(g) 07/03/2023 3:30*

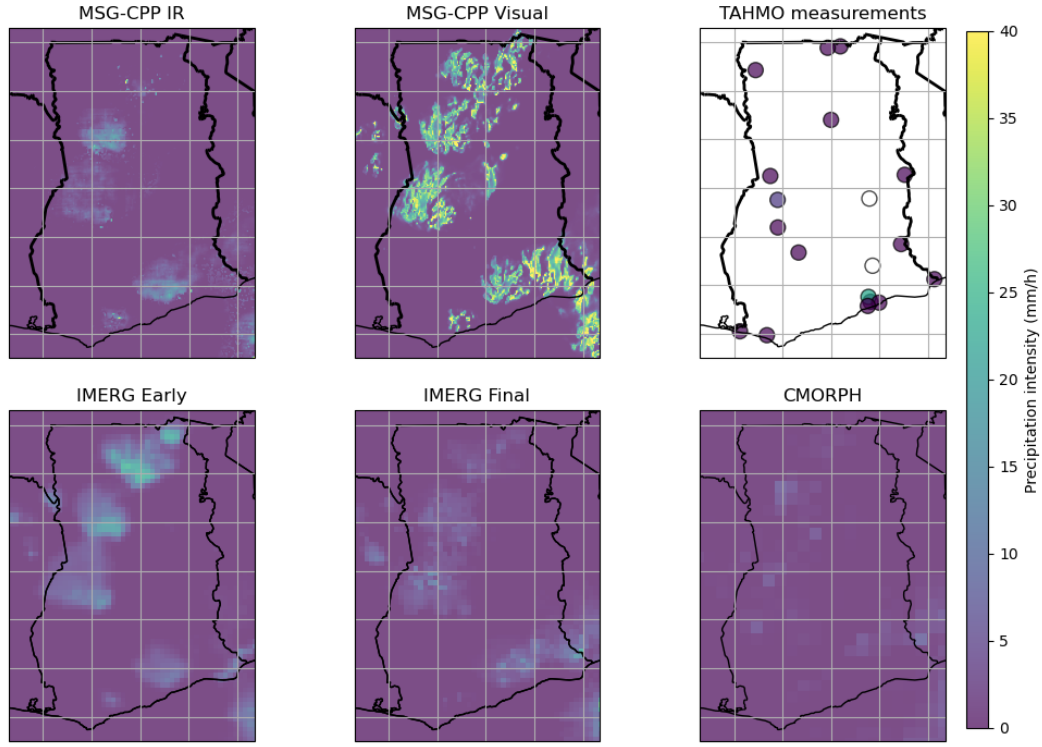


*(h) 27/04/2023 3:30*

***Figure A: Visual representation the selected precipitation events for various precipitation datasets***

# Appendix B: Precipitation intensity graphs of various retrieval products for the eight heavy precipitation events in Odaw basin

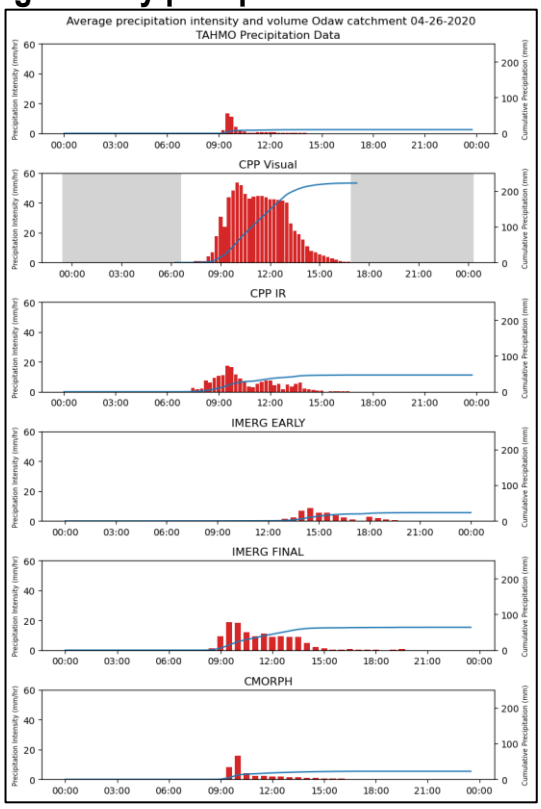


*(a) 04/26/2020*

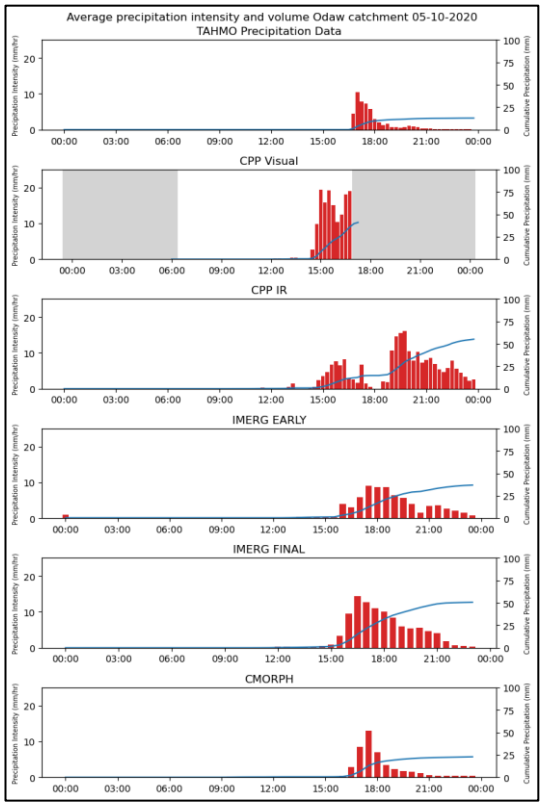


*(b) 10/05/2020*

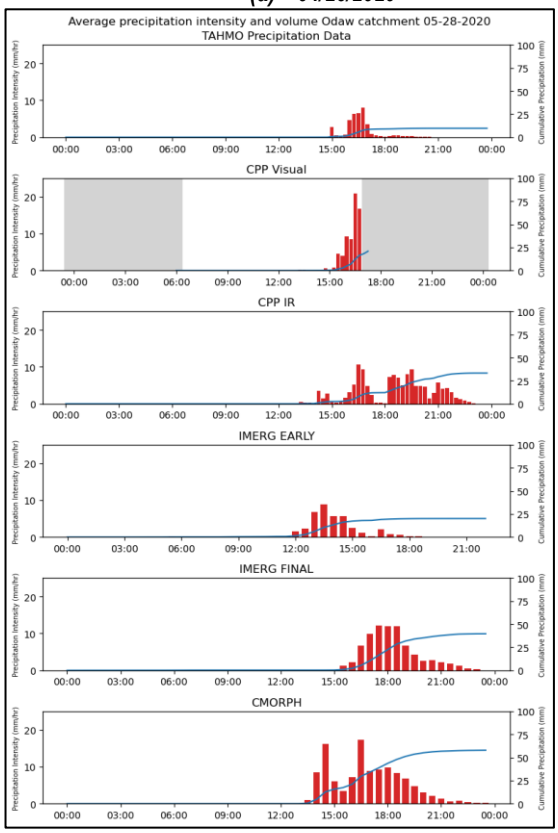


*(c) 28/05/2020*

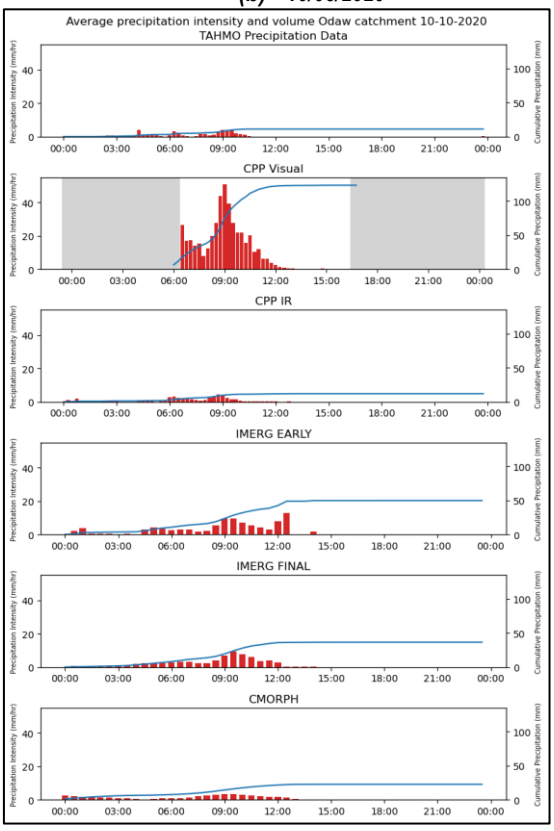


*(d) 10/10/2020*

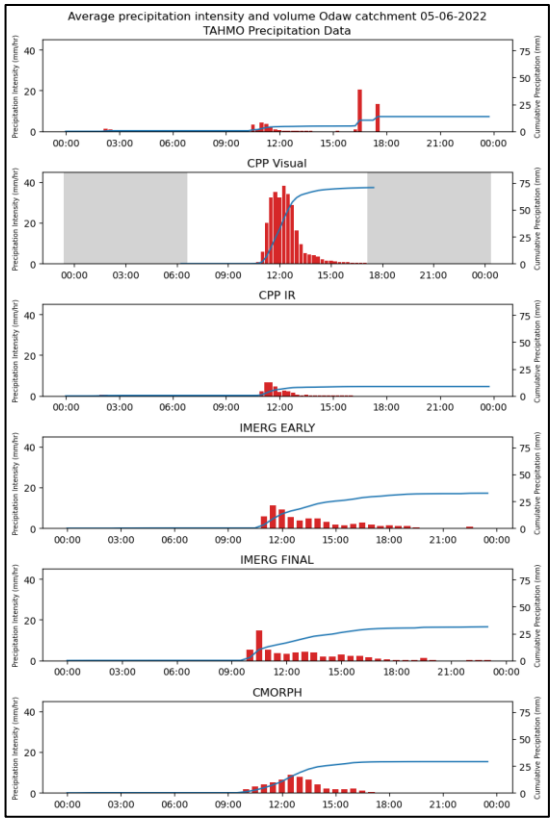


*(e) 06/05/2022*

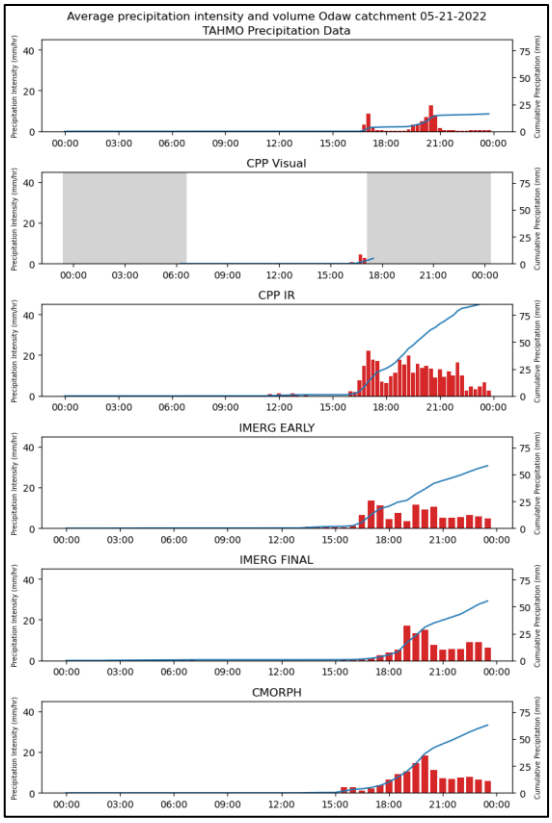


*(f) 21/05/2022*

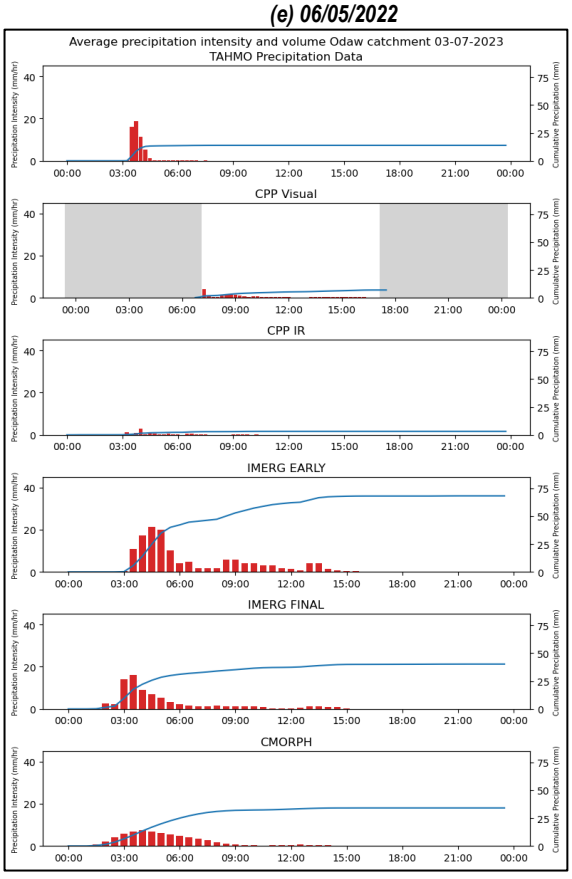


*(g) 07/03/2023*

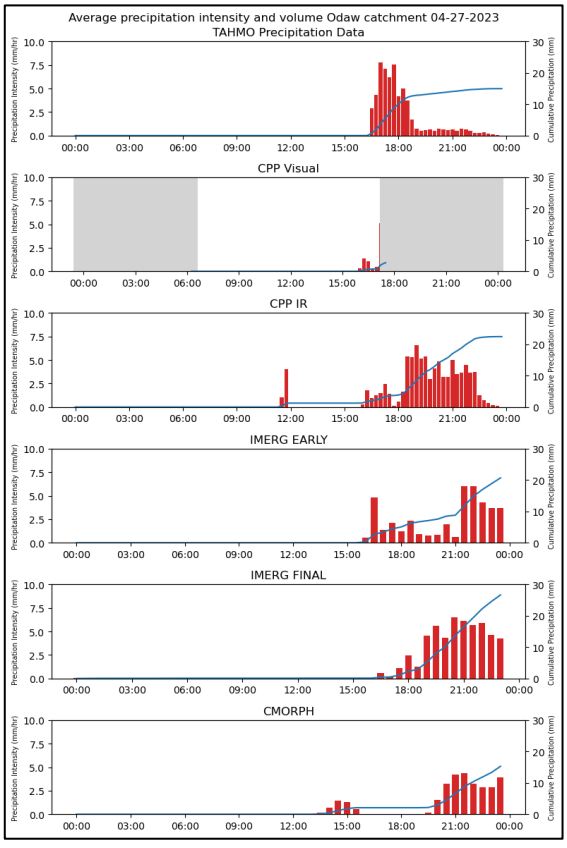


*(h) 27/04/2023*

***Figure B: Precipitation intensity graphs of eight heavy precipitation events for various precipitation data sources***

# Appendix C: Observed and nowcasted precipitation in Odaw basin for selected peak events and various temporal resolutions in input data

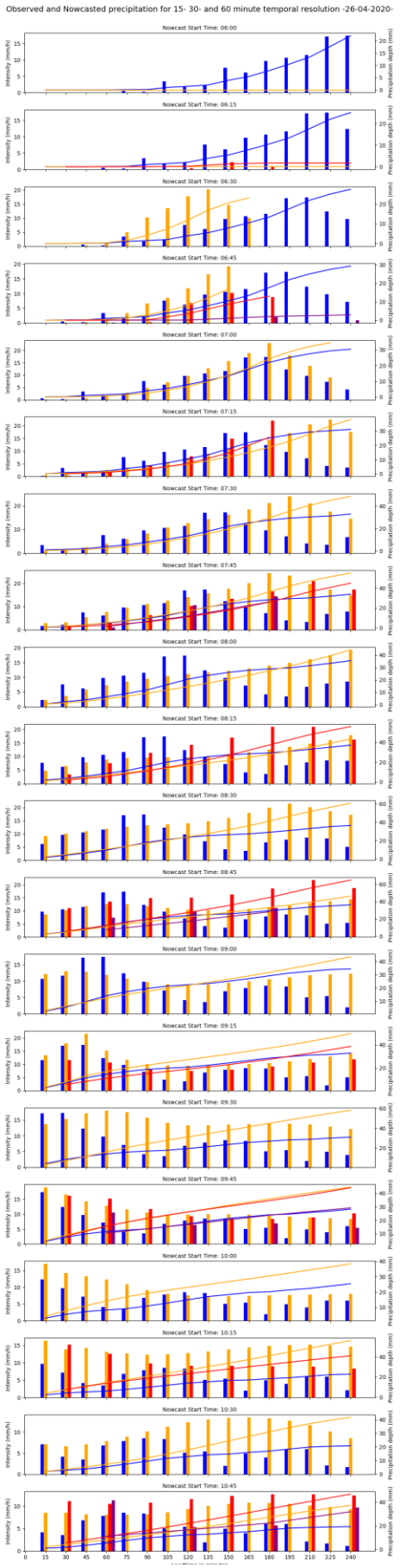


*(a) 26/04/2020*

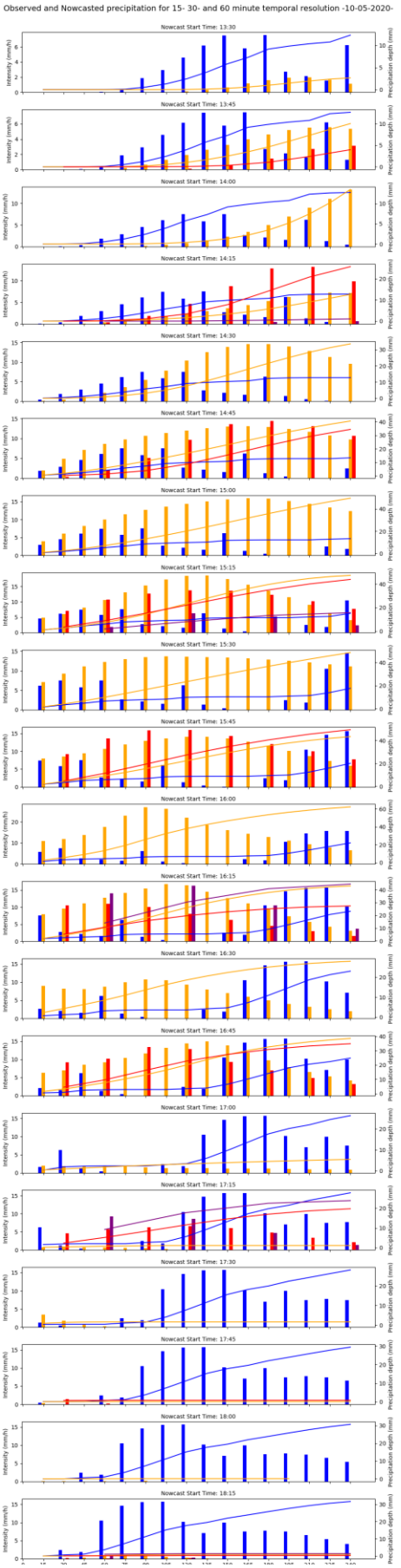


*(b) 10/05/2020*

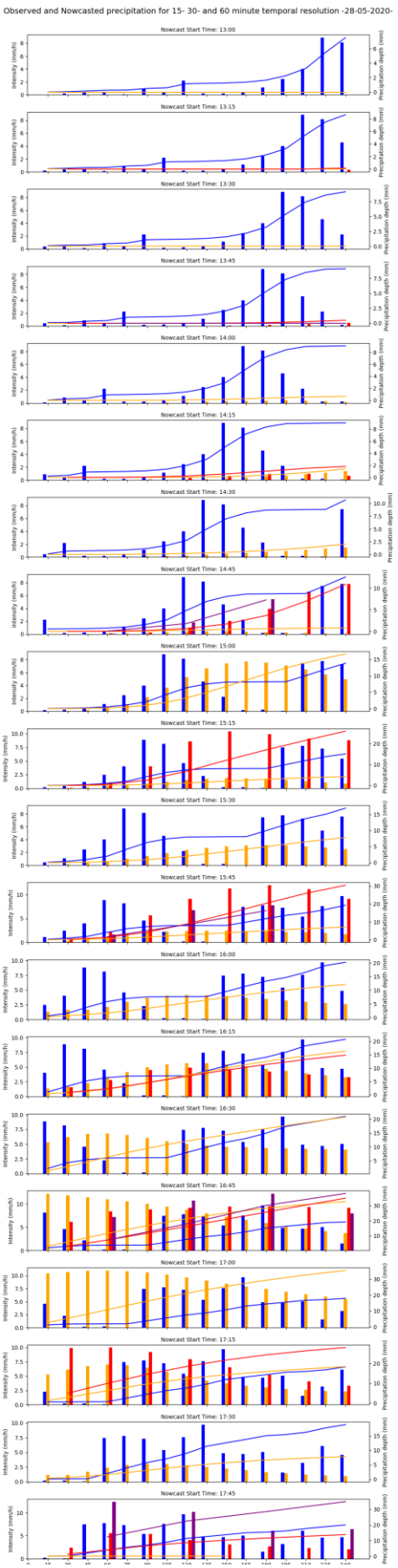


*(c) 28/05/2020*

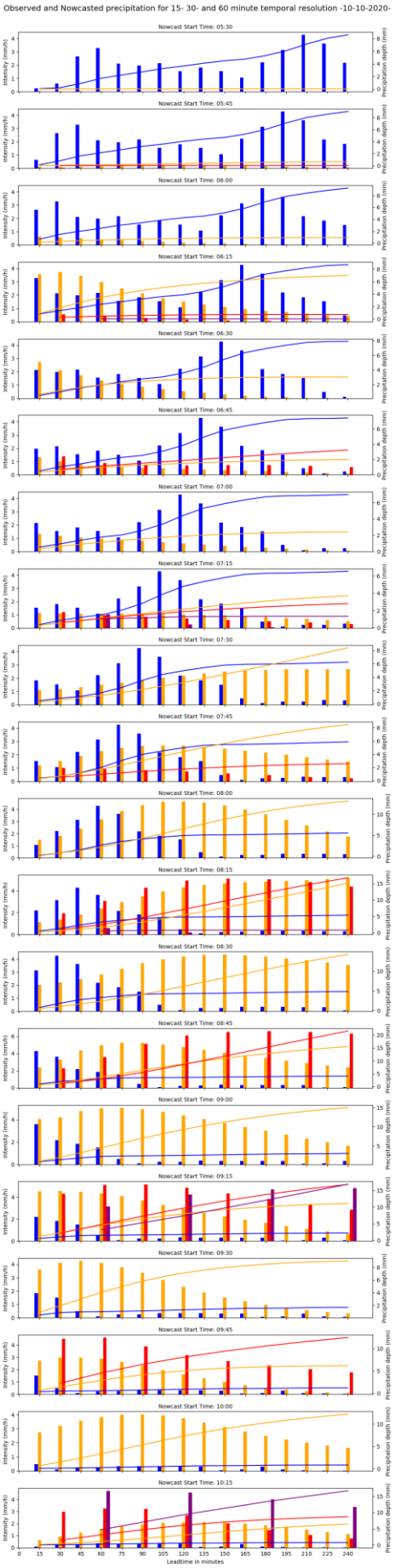


*(d) 10/10/2020*

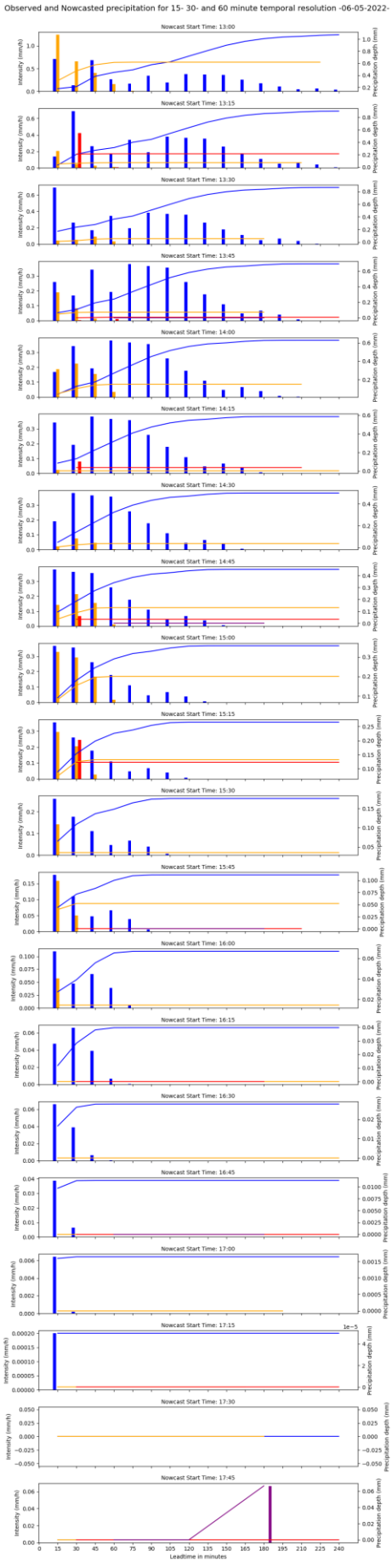


*(e) 06/05/2022*

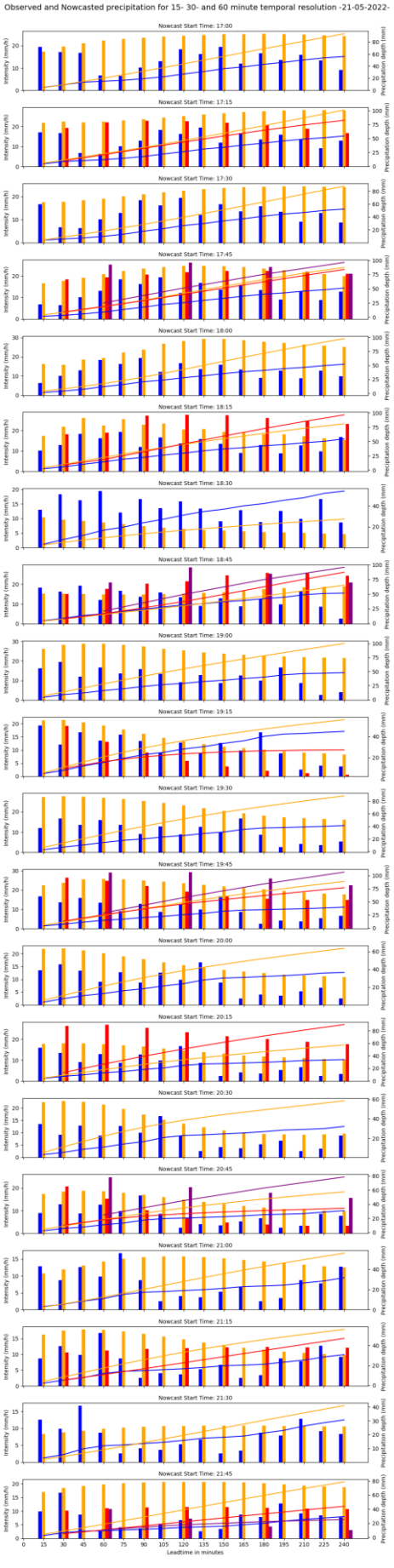


*(f) 21/05/2022*

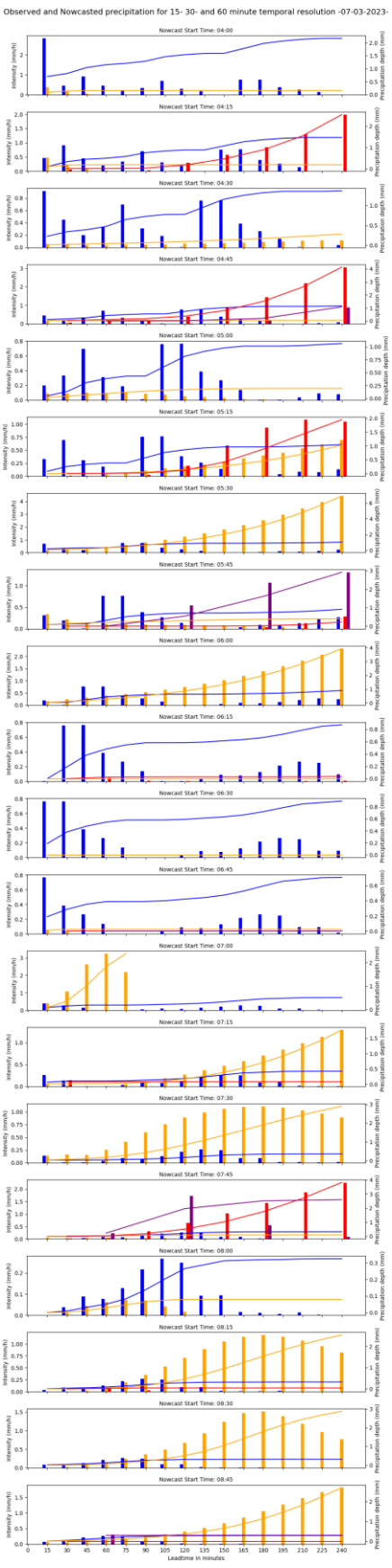


*(g) 07/02/2023*

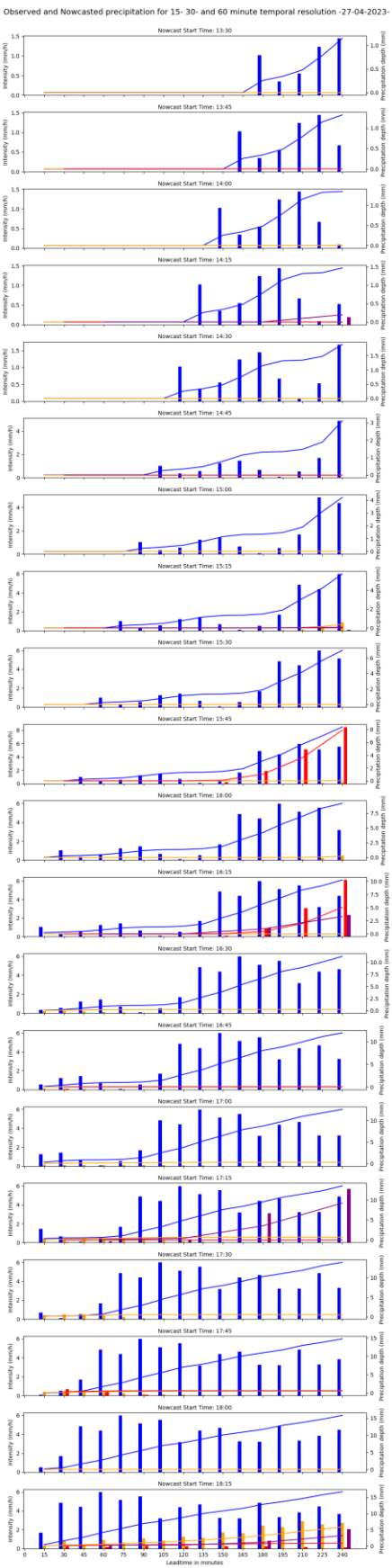


*(h) 27/04/2023*

***Figure C: Precipitation intensity graphs of observed (blue), nowcasted 15 min (yellow), nowcasted 30 min (red) and nowcasted 60 min (purple) temporal resolution of MSG-CPP IR input data and the associated cumulative precipitation***